# THE EFFECTS OF LOW-LEVEL WIND SHEAR ORIENTATION, DEPTH, AND MAGNITUDE ON LOW-LEVEL ROTATION IN SIMULATED SUPERCELL THUNDERSTORMS

A Thesis

by

FELICIA ROSE GUARRIELLO

Submitted to the Office of Graduate and Professional Studies of
Texas A&M University
in partial fulfillment of the requirement for the degree of

MASTER OF SCIENCE

| | |
|---|---|
| Chair of Committee, | Christopher Nowotarski |
| Co-Chair of Committee, | Craig Epifanio |
| Committee Members, | Robert Hetland |
| Head of Department, | Ping Yang |

August 2016

Major Subject: Atmospheric Science

# ABSTRACT

Supercell thunderstorms simulated using the numerical model CM1 are used to analyze the effects of low-level vertical wind shear on near-ground rotation in the storm. In particular, the parameters being assessed are the orientation, magnitude, and depth of the low-level vertical wind shear. Particular emphasis is given to the effects of the shear in determining the position of the low-level outflow relative to the midlevel mesocyclone/updraft.

The simulations are initialized using idealized soundings of quarter-circle, clockwise turning, with unidirectional westerly shear above 2 km hodographs. A control simulation is run without any low-level vertical wind shear to compare to the other runs. Experiments are then conducted in which the background sounding is modified by adding a low-level shear layer at one of three different orientation angles: 0° (easterly shear), 90 ° (southerly shear), or 180 ° (westerly shear).

Comparing a set of simulations run for a shear layer depth of 500 meters with a shear magnitude of 7 m $s^{-1}$, the most favorable orientation for intensifying near-ground rotation based on positioning of the outflow relative to the midlevel mesocyclone was the 0° case. The 90° case became more favorable after being run for another hour, where as the control and 180° cases did not develop favorable conditions. Changing the shear layer depth to 250 meters gives similar results, but when the shear layer depth is changed to 1 kilometer the most favorable simulation became the control. Finally, when the magnitude of the shear was increased to 15 m $s^{-1}$,

none of the cases was found to be favorable, as the outflow was not found to be positioned in any of the simulations below the midlevel mesocyclone.

Statistically, a significant negative correlation was found between the maximum near-ground vertical vorticity/circulation and the distance between the maximum near-ground rotation and the midlevel mesocyclone. When this distance decreased, the vertical vorticity/circulation increased, suggesting that the positioning of the outflow beneath the midlevel mesocyclone plays a key role in amplifying the surface rotation. For the particular sounding used in this study, a low-level shear orientation produces the most favorable positioning of the outflow beneath the mesocyclone, and thus lead to the strongest surface rotation among the cases considered.

First and foremost to my mom, Ann, and my dad, Tony, who were always there for me and taught me that I could do anything I set my mind to. To my sisters, Heather and Robyn, for accepting and fueling the nerd in me. Finally, to all the friends I've made over the last six years, for their constant support and all the amazing memories I will cherish forever.

# ACKNOWLEDGMENTS

This study was funded by NSF grant AGS-1446342. Thank you to my thesis committee: Christopher Nowotarski, Craig Epifanio, and Robert Hetland. A special thanks to my adviser Christopher Nowotarski for all the advice ,help along the way, and most importantly the countless hours spend reading over my thesis drafts. A huge thank you goes to George Bryan for developing and maintaining CM1.

# NOMENCLATURE

| | |
|---|---|
| AGL | Above ground level |
| CAPE | Convective available potential energy |
| FFD | Forward flank downdraft |
| HRRR | High-Resolution Rapid Refresh |
| LCL | Lifting condensation level |
| NSSL | National Severe Storms Laboratory |
| RFD | Rear flank downdraft |
| SPC | Storm Prediction Center |
| SREH | Storm Relative Environmental Helicity |
| SRW | Storm-relative winds |
| VPPGF | Vertical perturbation pressure gradient force |

# TABLE OF CONTENTS

# LIST OF FIGURES

# LIST OF TABLES

# 1 INTRODUCTION

Among the most dangerous types of convective storms is the supercell, which consists of a single, long-lived convective cell featuring a rotating updraft, or mesocyclone. Supercells are often associated with several different types of severe weather, including hail, flooding, high winds, and tornadoes. While not usually associated with a large number of deaths, hail and high winds cause large amounts of monetary losses through collapsing buildings and wind-driven debris (Cutter, 2001).

In addition to other hazards, supercells have drawn significant research attention because of their ability to produce tornadoes (e.g., Browning 1964, Lemon and Doswell 1979, Weisman and Klemp 1986, Bunkers et al. 2000, Markowski et al. 2003, Coffer and Parker 2015). According to Johns and Doswell (1992), most significant ($\geq$ EF2) and violent ($\geq$ EF4) tornadoes are produced by supercells, with supercell tornadoes accounting for a large majority of all tornado-related damage, injuries, and deaths. There are, on average, 60 tornado-related deaths each year in the US, caused by an average 1300 tornadoes (Edwards, 2000). Though conditions are most favorable in the central and southern US in spring and early summer, tornadoes can happen year round and can occur in many different locations in the United States and throughout the world. Thus, accurately forecasting them is of the utmost importance.

Forecasting when supercells will occur has improved throughout the years, but

forecasting which supercells will produce tornadoes is still a challenge, in part because tornadogenesis is not fully understood. It is generally known what environments typically result in supercells. The two most important parameters in a supercell environment are deep-layer (0-6 km) vertical wind shear and convective available potential energy (CAPE) (Moller et al., 1994). Vertical wind shear is associated with horizontal vorticity which is vital for midlevel updraft rotation. CAPE is also an important parameter and is usually high in supercell environments, although not always. (Moller et al., 1994)

The biggest uncertainty in supercell tornadogenesis is how rotation develops near the ground and is is subsequently amplified to tornado strength (Davies-Jones 2006, Markowski and Richardson 2009). Several environmental parameters (e.g., storm relative helicity, lifting condensation level (LCL), low-level shear) have skill in discriminating between tornadic and nontornadic supercells, but there is some overlap in values, particularly for weakly tornadic supercells (e.g., Markowski et al. 2003, Thompson et al. 2003, Esterheld and Giuliano 2008).

Another problem arises from radar detection and observation, which is a common tool used in forecasting. Most of the time radars cannot resolve tornadoes, they can only resolve the parent circulation (Markowski and Richardson, 2009) and only one in every four radar-detected mesocyclones are actually associated with tornadoes (Trapp et al., 2005).

While tornadic supercells are difficult to forecast, there are some methods that

show promise. There are high-resolution models [e.g. High-Resolution Rapid Refresh Model (HRRR) (Benjamin et al., 2016)] that help forecast potentially tornadic supercells hours to days in advance. While these models cannot yet resolve tornadoes, just mesocyclone-scale updraft helicity, they do help assist forecasters in making critical decisions. Two environmental parameters show promise in differentiating between tornadic and nontornadic environments as well. High low-level (the lowest 1 km AGL) shear has been shown to be a good discriminator (e.g. Markowski et al. 2003, Thompson et al. 2003, Craven and Brooks 2004), along with low lifting condensation level (LCL) (e.g. Rasmussen and Blanchard 1998, Thompson et al. 2003, Craven and Brooks 2004).

In this study, focus is placed on understanding the link between supercell environments and tornadogenesis with a goal of one day helping to create a better forecast. Though it in known that LCL and low-level shear are good predictors of tornadic supercells, it is still not fully understood why. If the dynamical link between these environmental parameters and supercell tornadoes was better understood, the information from the near storm environment could be used more effectively. For the present study, focus is placed on low-level shear; specifically, it is proposed to analyze how the depth, orientation, and magnitude of low-level shear can affect maturing supercells using idealized numerical simulations. The hypothesis focuses on how the low-level shear affects the positioning of the circulation-rich outflow with respect to the midlevel mesocyclone. There may be an ideal positioning of the outflow

relative to the midlevel mesocyclone where the convergence within the outflow will be optimized such that the vertical vorticity may be intensified. A more in-depth discussion the objectives and hypothesis can be found at the end of Chapter II.

Chapter II will provide background information on subjects useful to this study and review the thesis objectives and hypothesis. Chapter III will describe the numerical model configuration and the project methodology. The results and discussion of this study are presented in Chapter IV with conclusions presented in Chapter V.

# 2 BACKGROUND

## 2.1 Supercells

The first proposed kinematic model of a supercell was presented by Keith Browning in 1964 (Fig. 2.1), although Browning first used the term in his 1962 paper (Browning and Ludlam 1962). When the supercell was first identified, it was associated with storms with unusually long lifespans, but today a supercell is usually categorized by the presence of a persistent, deep rotating updraft (i.e., mesocyclone). Browning's model defines a supercell in two parts; an updraft with measurable rotation and a single downdraft, ahead of the updraft, within the precipitation region (Browning, 1964). Today, the model presented by Lemon and Doswell (1979) is the most widely used (Fig. 2.2). This model is based upon the model by Browning, but adds a second downdraft behind the updraft.

A supercell generally begins its life as a single cell, non-severe thunderstorm

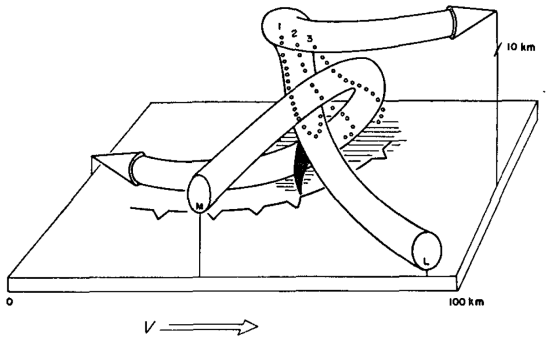


Figure 2.1: Three dimensional model of airflow within a supercell presented by Browning [Figure 2 from Browning (1964)]

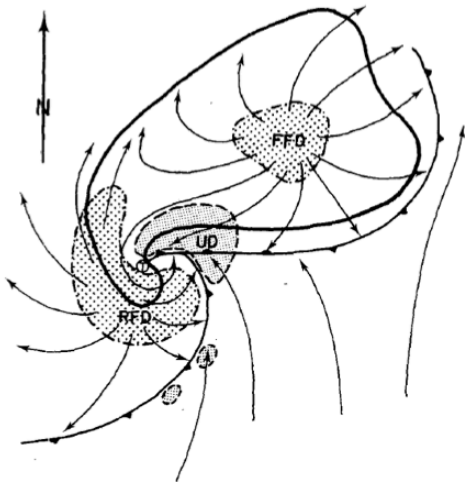


Figure 2.2: Schematic diagram of a tornadic supercell at the surface. A gust front can be seen and the radar echo is enclosed by the thick black line. The rear flank downdraft (RFD) and the forward flank downdraft (FFD) can also be seen upwind and downwind of the supercell's updraft. [Figure 7 from Lemon and Doswell (1979)]

(Lemon and Doswell, 1979). Strong, deep-layer vertical wind shear is crucial for the development and maintenance of the supercell updraft as well as the initiation of rotation. The environmental vertical wind shear is associated with horizontal vorticity, and as the storm develops, vorticity will be tilted into the vertical by the updraft, causing it to rotate. As the updraft strengthens, water begins to condense and once the condensed water becomes heavy enough to escape the updraft, it falls out as precipitation. This falling precipitation initiates a downdraft (Rogers and Yau, 1989) at a critical point in a supercell life cycle. If the vertical wind shear is not strong enough to displace the precipitation, it will fall into the updraft and cut off the updraft's positively buoyant inflow, effectively killing it. The wind shear needs to be intense enough to horizontally displace the downdraft. Figure 2.3 shows the structure of a mature supercell, and more detailed descriptions can be found in

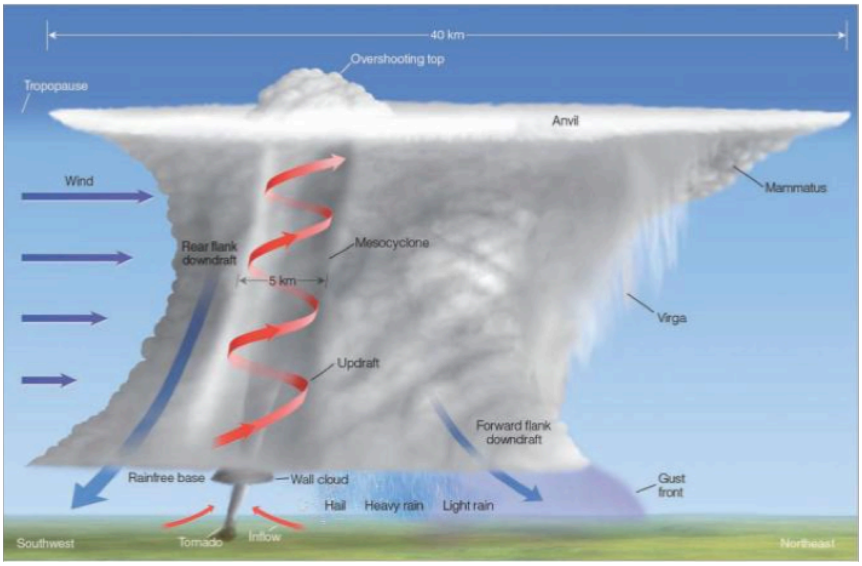


Figure 2.3: Some features of a mature supercell. The storm is moving to the northeast. [Figure 14.9 from Ahrens (2009)]

Weisman and Klemp (1986), Davies-Jones (2006), and Markowski and Richardson (2009).

While the formation process of a supercell is relatively well understood, tornadogenesis remains unclear. Supercell tornadogenesis can be examined as a three-step process. These steps are:

1. Development of midlevel rotation,
2. Near-ground (<100 m AGL) rotation development
3. Intensification of near-ground rotation to tornado strength

Each of these steps are examined below.

## 2.2 Development of Midlevel Rotation

The first step in the supercell tornadogenesis process is the development of midlevel rotation, also known as a midlevel mesocyclone. For midlevel rotation to develop, there must first be an adequate amount of vertical vorticity. The creation of vertical vorticity is achieved by the updraft tilting horizontal vorticity associated with the mean vertical wind shear (e.g., Rotunno 1981, Lilly 1982, Davies-Jones 1984, Rotunno and Klemp 1985). This tilting produces a vorticity couplet that straddles the updraft with positive (cyclonic) vertical vorticity on the right and negative (anticyclonic) vertical vorticity on the left if looking downshear. Equation 2.1 (Markowski and Richardson, 2009) shows the vertical vorticity tendency in the storm-relative reference frame. In this equation $\bar{\mathbf{v}}$ is the environmental horizontal velocity, which can be split into its i and j counterparts ($\bar{\mathbf{v}} = \bar{u}i + \bar{v}j$). $(\bar{\mathbf{v}} - \mathbf{c})$ is the storm-relative wind with $\mathbf{c}$ defined as the constant storm motion. If $\zeta'$ is the perturbation vertical vorticity (which we assume is the total vertical vorticity because the background vertical vorticity is ignored) then $\bigtriangledown_h \zeta'$ is the horizontal gradient of vertical vorticity. The mean vertical wind shear is represented by $\mathbf{S}$ ($\mathbf{S} = \frac{\partial \bar{\mathbf{v}}}{\partial z}$), the perturbation vertical velocity (which is, like the vertical vorticity, assumed to be the total) is $w'$, and $\mathbf{k}$ represents the vertical unit vector. The advection term can be seen in term (a) and the tilting term can be seen in term (b).

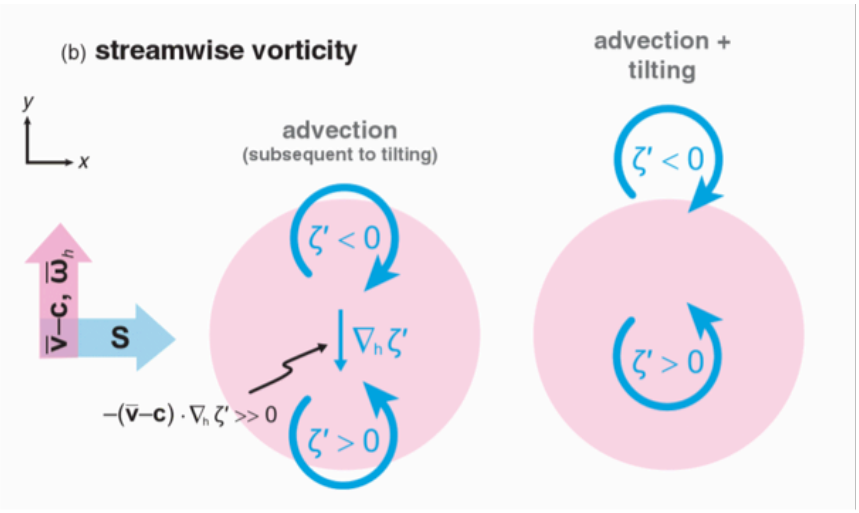


Figure 2.4: Evaluation of storm-relative vertical vorticity via the advection term based on the fact that the tilting term leads to a couplet of vertical vorticity straddling the updraft and oriented normal to the shear vector for the case of streamwise vorticity. See equation 2.1. [Figure 8.30 from Markowski and Richardson (2011)]

$$\left(\frac{\partial \zeta'}{\partial t}\right)_{sr} = \underbrace{-(\bar{\mathbf{v}}-\mathbf{c}) \cdot \nabla_h \zeta'}_{\text{(a) advection}} + \underbrace{\mathbf{S} \times \nabla_h w' \cdot \mathbf{k}}_{\text{(b) tilting}} \tag{2.1}$$

Once the vertical vorticity has developed through tilting, advection by the storm-relative winds (Eq. 2.1(a)) can shift the vertical vorticity field horizontally relative to the storm updraft. If the storm relative winds (SRW) are in the same direction as the environmental horizontal vorticity (i.e., streamwise vorticity), the cyclonic vortex will be advected towards the center of the updraft while the anticyclonic vortex will be shifted out of the updraft (Rotunno and Klemp, 1985).

After the vertical vorticity has been tilted and advected (Fig. 2.4), stretching may cause the vertical vorticity to intensify. This happens over the positive vertical vorticity that has been advected into the center of the updraft below the updraft

maximum. This is an important step in the development of midlevel rotation because the more the vorticity is stretched the more the rotation will intensify (Klemp, 1987). This process will cause midlevel rotation to develop, leading into the second step in supercell tornadogenesis.

### 2.3 Near-Ground Rotation Development

Often after a midlevel mesocyclone forms (though it is not necessary for one to exist), a supercell can go on to develop near-ground rotation. Before a tornado can form, vertical vorticity must be present at the ground (Davies-Jones et al., 2001). If there is preexisting vertical vorticity in large enough quantities at the surface, it can simply be amplified to tornado intensity by near-ground convergence. If, however, surface vertical vorticity is non-existent or is too small in magnitude, then it must first be generated in one of two ways:

1. Tilting of the preexisting or storm-generated horizontal vorticity, or
2. Advection of vertical vorticity toward the surface from aloft

Tilting of horizontal vorticity by an updraft alone does not cause near-ground rotation because the air is being moved away from the ground as it is being tilted (Markowski and Richardson, 2009). If this is the case, then a downdraft is needed. If a downdraft is present, the vertical vorticity can be advected towards the surface (Fig. 2.5e) as it is being generated through tilting. This allows vertical vorticity to be near the ground where it can be stretched to form a tornado (Markowski and

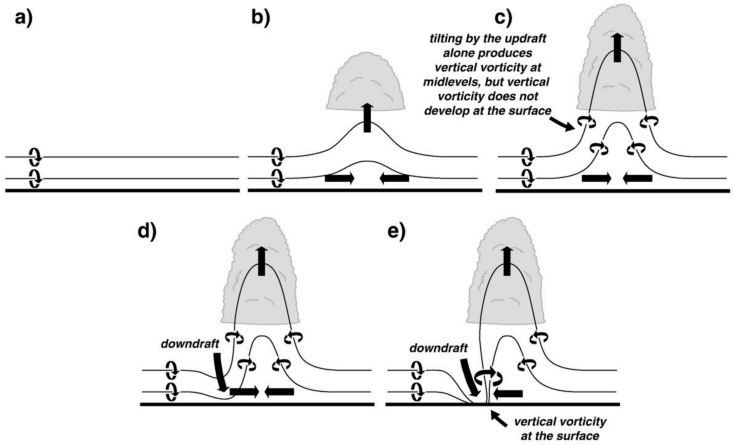


Figure 2.5: Simple vortex line demonstration of why a downdraft is needed in order for significant vertical vorticity to develop at the ground beneath a thunderstorm in the absence of preexisting vertical vorticity at the surface. (a)–(c) Evolution of vortex lines as a result of tilting by an updraft alone. (d)–(e) Possible evolution of vortex lines following the formation of a downdraft. [Figure 2 from Markowski and Richardson (2009)]

Richardson, 2009).

Baroclinic generation of horizontal vorticity within a downdraft may be important in the process of developing rotation near the ground. This can be seen conceptually when analyzing vortex lines. Vortex lines in the vicinity of low-level mesocyclones form arches that join counter rotating vortices on opposite sides of the rear-flank downdraft (RFD) (Markowski et al. 2008, Markowski and Richardson 2009). Markowski et al. (2008) concluded that "the arching of the vortex lines and the orientation of the vorticity vector along the vortex line arches...are strongly suggestive of baroclinic vorticity generation within the hook echo and associated RFD region of the supercells, and subsequent lifting of the baroclinically altered vortex lines by an updraft". This process helps produce a low-level vorticity maximum.

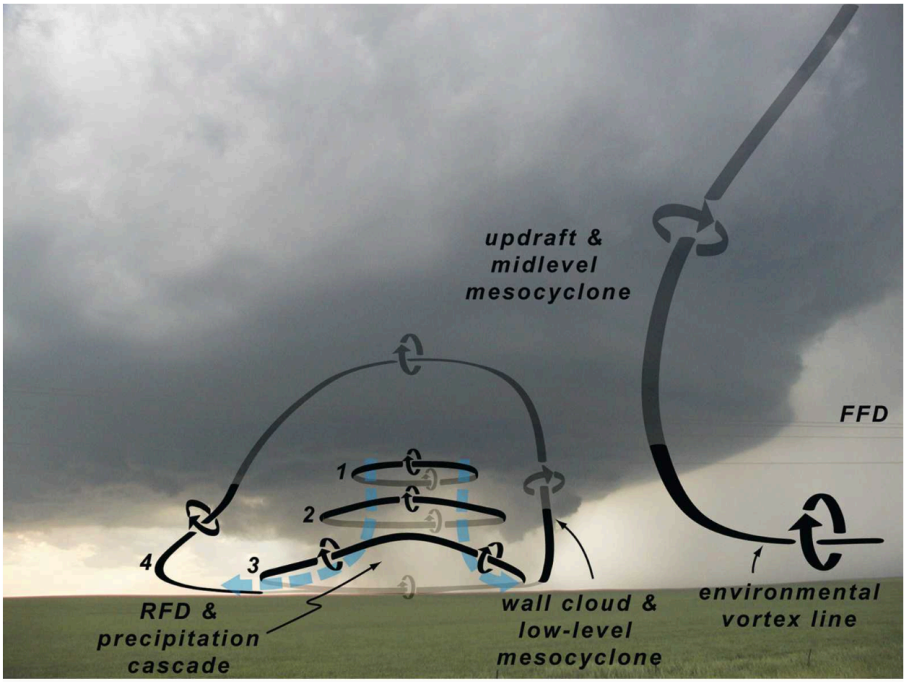


Figure 2.6: Evolution of vortex rings and arches. 1–4 are the vortex lines at different stages of evolution. [Figure 19 from Markowski et al. (2008)]

Figure 2.6 shows this process further.

Because of the role of baroclinic vorticity generation within a downdraft, near-ground rotation tends to develop in the cold, usually negatively buoyant, outflow air. Once the low-level rotation has developed, it can be intensified to tornado strength, given the right conditions.

## 2.4 Intensification of Near-Ground Rotation to Tornado Strength

In order for near-ground rotation to intensify, convergence is needed. Beneath the dynamically induced low-level updraft, vorticity is converged and begins to intensify in its rotation. It is hypothesized that the midlevel mesocyclone needs to be located over the near-ground circulation for the convergence/stretching to occur

because of the need for dynamic lifting of negatively buoyant outflow air.

There is still much to learn when it comes to the intensification of low-level rotation to tornado strength, but there are several hypotheses presented in an attempt to better explain how the storm environment modulates the process. One hypothesis is stated in Markowski and Richardson (2014), although they are not the first to suggest it (e.g., Davies-Jones 1982), who connect the large low-level vertical wind shear to the strength of the dynamic forcing. They state that increased streamwise vorticity near the ground leads to a stronger midlevel mesocyclone, which lowers the pressure through non-linear dynamic effects, thereby enhancing the low-level, upward-directed dynamic vertical perturbation pressure gradient force and subsequent convergence of near-ground vertical vorticity. This can be seen in Figure 2.7, which shows dynamic lifting for both a weak shear case (left) and a strong shear case (right). This figure shows the importance of low-level wind shear to the strength of the dynamic lifting. The strong shear has a much larger value of dynamic lifting than the weak shear, allowing for much stronger low-level rotation to develop.

In the same paper, Markowski and Richardson also address the intensification of low-level rotation in relation to cold pools and low-level relative humidity (RH). Tornadogenesis is more likely to occur in supercells with weak (less negatively buoyant) cold pools (Markowski and Richardson, 2014). The small negative buoyancy of circulation-rich air combines with the strong midlevel updraft, which aides low-level vorticity stretching. Because outflow is generally negatively buoyant, any updraft

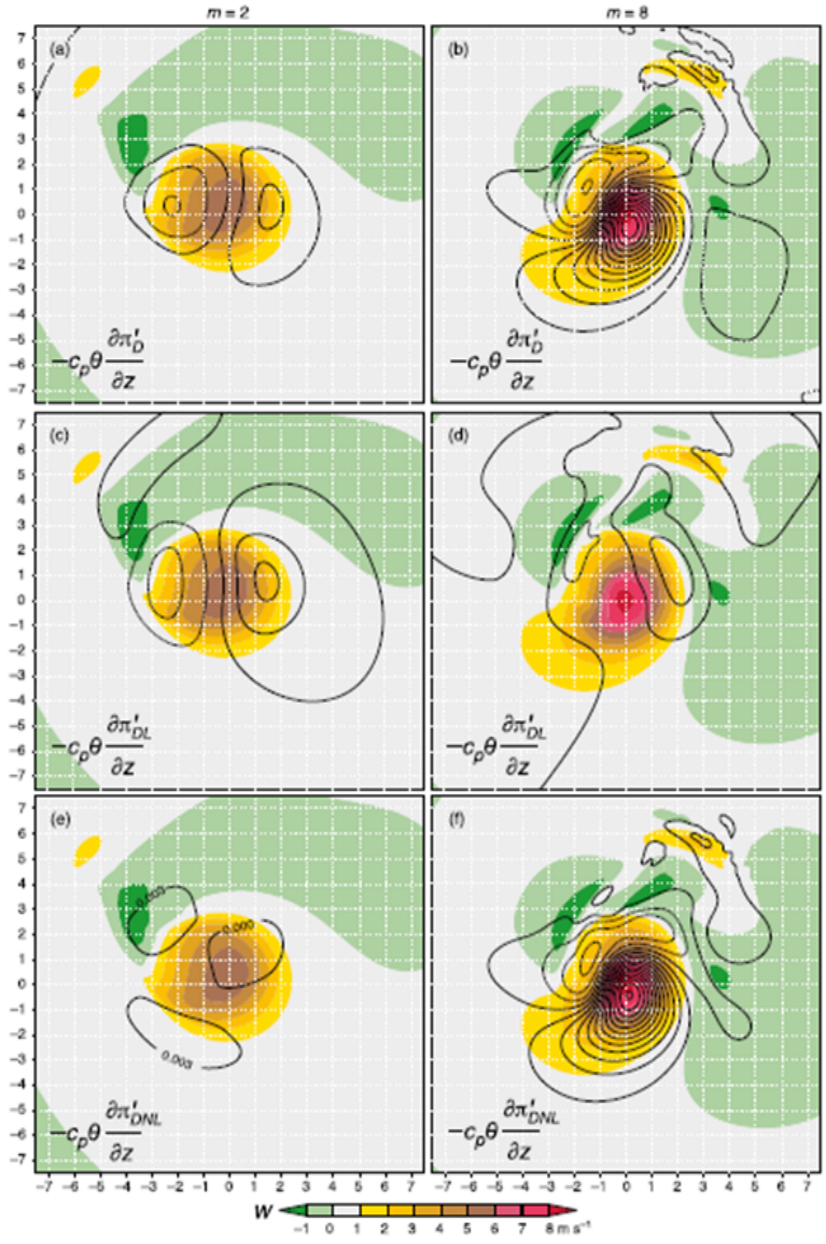


Figure 2.7: Horizontal cross sections of 0–1 km mean vertical perturbation pressure gradient force (VPPGF). (a)and(b) are dynamic, (c) and (d) are linear dynamic, and (e) and (f) are nonlinear dynamic. The panels on the left are weak shear and the panels on the right are strong shear. [Figure 4 from Markowski and Richardson (2014)]

and associated convergence/stretching has to be dynamically driven. The less negatively buoyant the outflow, the easier it is to dynamically lift because there is less negative buoyancy to overcome.

## 2.5 Discriminating Between Tornadic and Nontornadic Supercells

Previous research has shown that low-level wind shear and LCL can discriminate between tornadic and nontornadic supercells (e.g. Thompson et al. 2003, Craven and Brooks 2004, Markowski and Richardson 2009). Vertical wind shear, over a 0-1 km layer, has been shown to be much stronger in severe tornadic environments versus nontornadic environments (Fig. 2.8), having a difference as large as up to 10 m/s (Thompson et al., 2003).

Along with varying magnitude differences, the shear layer over which the magnitude is calculated is another factor in discriminating between environments. Several studies have looked at different layers, and most came back with the same conclusion, that differences become more apparent when looking in the lowest 1 km of the storm environment (e.g., Brooks and Craven 2002, Markowski et al. 2003, Thompson et al. 2003, Craven and Brooks 2004, Esterheld and Giuliano 2008).

Another factor that could be significant is low-level shear orientation. Thompson and Edwards (2000) analyzed a tornado outbreak that occurred in May 1999. While studying the outbreak they noted that in the environments of supercells producing significant tornadoes the angle between the speed shear and the directional

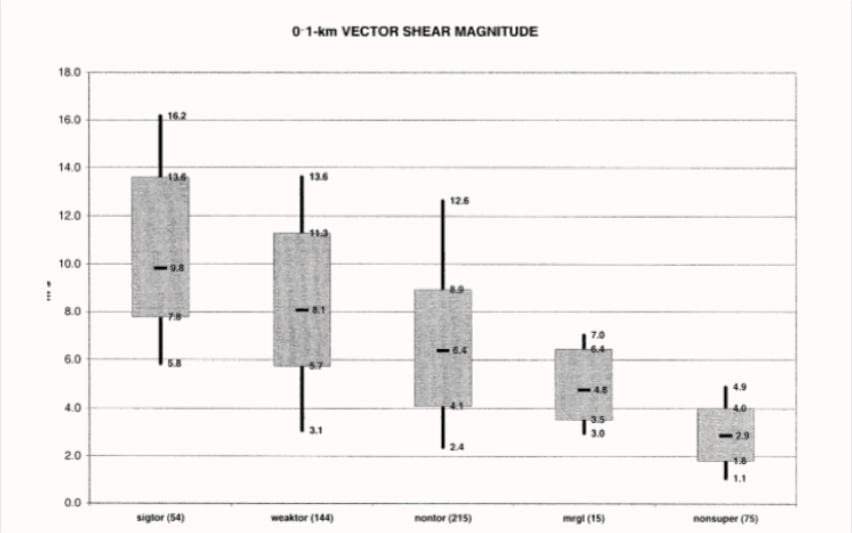


Figure 2.8: Box and whiskers plot of 0-1 km vector shear magnitude (m $s^{-1}$) values. Shown are significantly tornadic supercells (sigtor), weakly tornadic supercells (weaktor), nontornadic supercells (nontor), "marginal" supercells (mrgl), and discrete nonsupercell storms (nonsuper). The shaded box covers the 25th-75th percentiles, the whiskers extend to the 10th and 90th percentiles, and the heavy horizontal line within each shaded box marks the median values. [Figure 9 from Thompson et al. (2003)]

shear varied. This "hodograph kink" was not analyzed any further, but a note was made about the possibility of discriminating between weak and strong tornadic supercells. Another study by Parker (2014), who analyzed 67 different severe weather events, found that the most favorable hodograph shape in the lowest levels for tornadic supercells was characterized by a 90° angle.

A more recent study (Esterheld and Giuliano, 2008) also explored the idea that the low-level shear critical angle (defined as the angle between a hodograph's 10-500 m bulk shear vector and the 10 m inflow vector) discriminates between tornadic and nontornadic supercells. In the study, Esterheld and Giuliano analyzed 67 severe events separated into non-tornadic, weak-tornadic, and strong-tornadic cases.

In comparing these events it was found that the critical angle most favorable for tornadogenesis was 90°. More weak-tornadic cases have 90° critical angles than any other critical angle, while strong-tornadic had an overwhelming amount of 90° critical angle cases. Non-tornadic supercells appeared to favor 110°.

Along with various low-level vertical wind shear parameters, low LCLs (high boundary layer relative humidity) have been found to be the most favorable for tornadic environments (Craven and Brooks, 2004).

## 2.6 Cold Pool and Low-Level Shear Interactions

Along with affecting the intensification of midlevel and low-level mesocyclone scale rotation, low-level shear interactions with the cold pool may also affect supercell near-ground rotation. Shear interactions with cold pools are often studied as they relate to squall line maintenance (e.g., Rotunno et al. 1988); however, much of the same dynamics may also be applicable to supercell cold pools.

In the context of squall line maintenance, without the presence of shear, the cold pool causes circulation near the ground, but the low-level air is swept up and over the cold pool, causing a lack of upward displacement, which is needed for convection (Fig. 2.9a). If there is low-level shear but no cold pool, the updraft will tilt downshear (Fig. 2.9b). This is problematic for supercells because it causes the downward-directed buoyancy pressure gradient force to increase which results in a smaller upward acceleration (Lilly, 1979). It is clear that the presence of both a cold

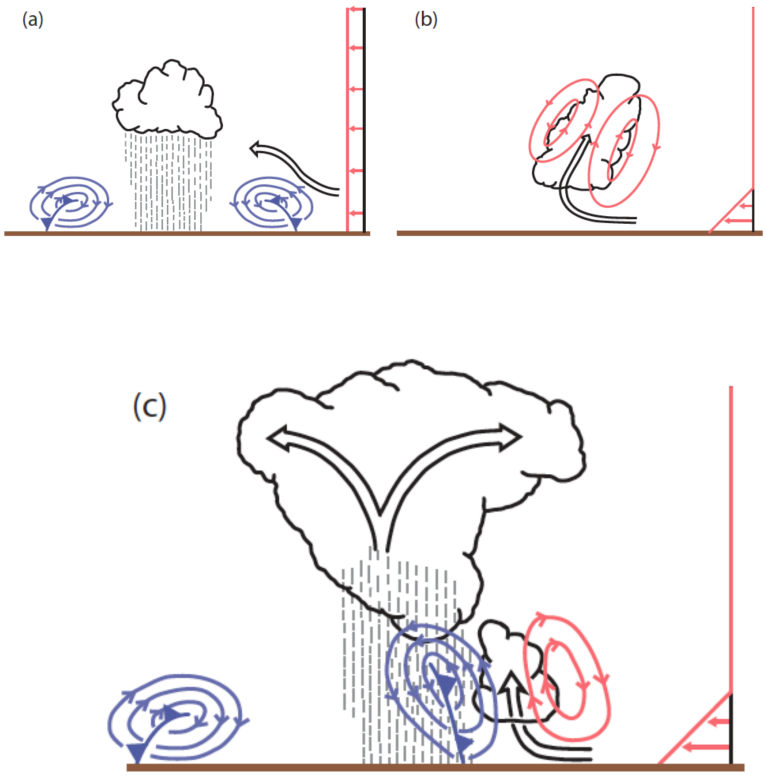


Figure 2.9: Interpretation of RKW theory. Panel (a): updraft with only a cold pool present, panel (b): updraft with only vertical wind shear present, panel (c): updraft with cold pool and vertical wind shear interaction. [Figure 5 from Bryan (2012)]

pool and low-level shear is necessary for multicell/squall line development. The two processes can offset each other on the downshear side of the cold pool (Fig. 2.9c).

If the low-level shear oriented perpendicular to the gust front is not strong enough, the cold pool can surge ahead and the storm will not be maintained, but if the low-level shear is too strong, the cold pool will be held back behind the storm. This can be seen in Figure 2.10, which shows a numerical simulation of an eastward-moving density current in an environment containing westerly wind shear, no wind shear, and easterly wind shear respectively. The shear can be seen having an effect

on the head of the density current, which, in turn, affects the strength and depth of the lifting that occurs there. If shear/cold pool dynamics do apply to supercells, the orientation of the shear vector may matter as much as the magnitude.

A study by Weisman and Rotunno (2004) reevaluates the theory put forth by Rotunno et al. (1988) on cold pool and shear interactions in squall line maintenance. They concluded that there is an optimal state of shear and cold pool strength that maintains the strongest squall lines. Not only that, but the orientation of the shear to the cold pool also has a large impact. Investigation into the extent to which shear/cold pool interactions affect rotation in supercells will be presented herein.

It is also possible LCL could affect cold pool density and propagation. James et al. (2006) found that there was a direct connection between LCL (mixed-layer relative humidity) and cold pool strength. A high LCL (lower mixed-layer relative humidity) leads to a stronger cold pool and the possibility of an outflow dominated storm. On the other hand, a low LCL leads to a weak cold pool, which could be over powered by shear.

Shear/cold pool interactions are important to this study as the near-ground rotation is in the cold pool. The cold pool position will then determine, in part, the relative position between the near-ground circulation and the midlevel mesocyclone.

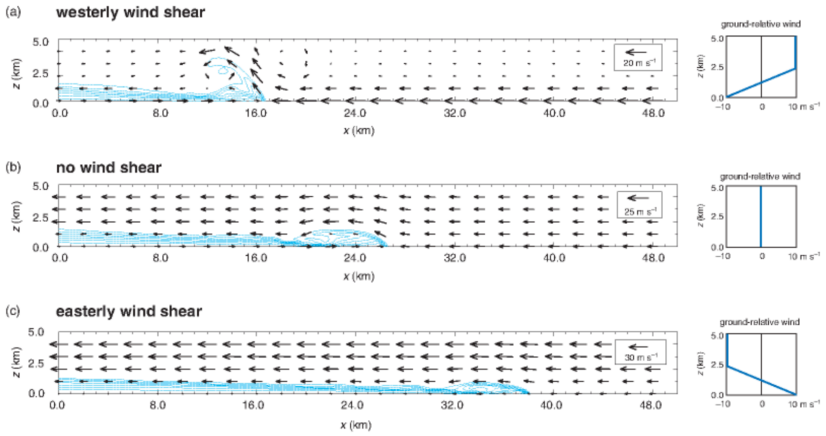


Figure 2.10: Numerical simulation of an eastward-moving density current in an environment containing (a) westerly wind shear, (b) no wind shear, and (c) easterly wind shear. Potential tamperature perturbations are contoured at 1 K intervals within the cold pool, starting at -1 K. Wind vectors are relative to the density current. The ground-relative wind profiles are shown for each case on the right. [Figure 5.31 from Markowski and Richardson (2011)]

## 2.7 Thesis Objectives and Hypothesis

From all the previous research done on discriminating between tornadic and nontornadic supercells, it is clear there is a connection between tornadic supercells and low-level wind shear. What we still do not know fully, however, is why this connection exists, or how these factors affect low-level rotation intensification to tornado strength.

There has been focus on an explanation for the effects of low-level shear magnitude on a supercell (Markowski and Richardson, 2009), but this explanation looks primarily at the strength of the dynamical forcing aloft. The position of the dynamic forcing may be just as important as its strength. If the dynamic forcing from the midlevel mesocyclone is not positioned correctly (above the near-ground circulation),

the near-ground circulation may not intensify to tornado strength. This means the orientation of the shear vector, not just its magnitude, should matter. Markowski and Richardson (2014) showed some effects that low-level shear and LCL had on the position of the dynamic forcing, but they did not focus on the effects it would have on near-ground circulation.

The objective of this study is to test a relatively unexplored hypothesis that considers the effects of low-level shear on the position of the near-ground, circulation-rich outflow, relative to the overlying midlevel mesocyclone. Based on previous studies and what is already known about supercell dynamics and tornado generation, it is hypothesized that the position of the outflow relative to the midlevel mesocyclone will be affected by the orientation and strength of the low-level winds and wind shear. In turn, there may be an ideal position of the near-ground, circulation-rich outflow relative to the midlevel mesocyclone where convergence within the outflow is optimized such that vertical vorticity is intensified. This hypothesis focuses on the positioning of the necessary dynamic forcing, rather than its strength.

Several questions will be addressed regarding the influence of low-level shear on rotation in supercell thunderstorms:

1. How do the direction, depth, and strength of low-level shear affect the magnitude of near-ground rotation?
2. Do changes in the low-level shear orientation, strength, and depth affect the properties and/or the positioning of supercell outflow relative to the midlevel

mesocyclone?

3. Does this relative positioning influence the strength of near-ground rotation?

Comparable to other studies that have looked at supercell dynamics (e.g., Klemp and Wilhelmson 1978, Klemp et al. 1981, Grasso and Cotton 1995, Dahl et al. 2014, Coffer and Parker 2015), an idealized numerical model will be used to explore the hypothesis. Using a numerical model allows the modeler to isolate the role of the low-level wind profile while keeping other parameters constant. It is idealized because none of the soundings that will be used are real life cases and they will be applied over a horizontally homogeneous domain; they are all created with the purpose of studying the effects of slight alterations in the low-level wind shear.

In this study, the focus will be placed on the intensification of near-ground rotation in supercells and the effect that low-level vertical wind shear has on this process. The specific low-level environmental wind parameters that will be varied are the depth over which the vertical wind profile is modified, the angle of the low-level shear vector with respect to the deep-layer wind profile, and the magnitude of the low-level shear vector.

# 3 METHODS

In order to maintain complete control over the environmental parameters that will be changed in each scenario, a numerical model shall be used. While numerical models cannot be considered truth when comparing to the actual atmosphere, there are many advantages to using this method of study.

One advantage is that the modeler has full knowledge of the parameters that are in the model and is able to adjust any one of them at will. The modeler also has access to a full range of data output. This is useful for this study as much emphasis is placed on the position of the supercell's outflow relative to the overlying midlevel mesocyclone and distance calculations between the maximum near-ground circulation and midlevel mesocyclone can be made using the wide range of output data. The modeler is able to isolate the low-level wind profile which is the basis for this study.

## 3.1 Numerical Model

The simulations for this study are performed using CM1 (cloud model 1), release 17 (Bryan and Fritsch 2002, Bryan 2014). CM1 is a three-dimensional, non-hydrostatic, time-dependent numerical model designed for idealized studies of atmospheric phenomena (Bryan, 2014). A method from Klemp and Wilhelmson (1978) is used to solve the compressible governing equations in this model.

In this configuration, the grid spacing used is 500 meters in the horizontal, with a stretched grid spacing used in the vertical. This stretched vertical grid allows for 50-meter grid spacing below 4 kilometers, increasing to 500 meter grid spacing above 15 kilometers.

In order to allow for a full view of the storm, there are 350 x 350 grid points in the horizontal and 130 in the vertical. Each simulation is run for three hours, with a large time step of 5 seconds, to allow each storm the time to mature. Data was output every five minutes so an accurate picture of what is happening can be established. An adaptive time step was also used in order for the model to maintain computational stability (Mansell, 2010). This feature allowed the model to adjust the small time step, which is used for solving terms that deal with acoustic waves (Klemp and Wilhelmson, 1978). A full list of specifications used can be seen in Table 3.1, which are used in each simulation run unless otherwise noted.

In regard to the boundary conditions, the top and bottom boundaries are rigid and free slip, while the lateral boundary conditions are open-radiative using a scheme from Durran and Klemp (1983). There is an upper-level Rayleigh damping zone which is applied above 15 km. The Morrison double moment microphysics parameterization (Morrison et al., 2005) is used with a sixth order diffusion scheme and a 1.5-order closure sub-grid turbulence scheme (Deardorff, 1980). Coriolis force is ignored in these simulations because of the relatively short time and spatial scales being studied.

Table 3.1: Table of model specifications for simulation runs.

| | |
|---|---|
| **Horizontal Grid Space** | 500 m |
| **Vertical Grid Space** | Stretched<br>50 m below 4 km<br>increased to 500 m above 15 km |
| **Horizontal Grid Points** | 350 x 350 |
| **Vertical Grid Points** | 130 |
| **Storm Motion** | (18,10) m $s^{-1}$ |
| **Run Time** | 10800 s (3 hrs) |
| **Frequency of Output** | 300 s (5 min) |
| **Boundary Conditions** | Top and Bottom: rigid and free slip<br>Lateral: Open-radiative |
| **Microphysics Parametrization** | Morrison double moment |
| **Sub-Grid Turbulence Scheme** | 1.5-order closure |
| **Storm Initialization** | warm bubble (max temp. 1 K) |
| **Model Top** | 20 km |
| **Rayleigh damping** | above 15 km |

An external file created by the modeler is being used for the base state sounding so that the parameters can be easily changed. Once the base state sounding is input into the model, the storm is initialized using a warm bubble with a maximum potential temperature perturbation of 1 K. The horizontal radius of the warm bubble is 10 km and the vertical radius is 1.4 km with the center of the warm bubble located 14 km above the surface.

## 3.2 Base States

### 3.2.1 Thermodynamic Profiles

The thermodynamic profiles remain the same for each simulation run so that the only factor changing is the wind profile. The thermodynamic soundings for each simulation were created with equations obtained from Weisman and Klemp (1982). The potential temperature and relative humidity were calculated by

$$\Theta(z) = \begin{cases} \Theta_{sfc} + (\Theta_{tr} - \Theta_{sfc})(\frac{z}{z_{tr}})^{5/4}, & z \leq z_{tr}. \\ \Theta_{tr} exp[\frac{g(z-z_{tr})}{c_p T_{tr}}], & z \geq z_{tr}. \end{cases} \tag{3.1}$$

and,

$$H(z) = \begin{cases} 1 - (1 - RH_{min})(\frac{z}{z_{tr}})^{5/4}, & z \leq z_{tr} \text{ and } z \leq z_{invb}. \\ RH_{k-1} - 0.0007dz, & z \leq z_{tr} \text{ and } z_{invb} \leq z \leq z_{invt}. \\ 1 - (1 - RH_{min})(\frac{z}{z_{tr}})^{5/4}, & z_{invt} \leq z \leq z_{tr}. \\ H = 0.50, & z \geq z_{tr}. \end{cases} \tag{3.2}$$

In the above equations, the surface potential temperature ($\Theta_{sfc}$) is 300 K and the tropopause potential temperature ($\Theta_{tr}$) is 343 K. The tropopause height ($z_{tr}$) is 12 km, with the tropopause temperature ($T_{tr}$) being 213 K. The relative humidity minimum ($RH_{min}$) is set to 0.50 and the vertical layers (dz) are 50 meters. The inversion layer top ($z_{invt}$) is set to 1750 meters with the inversion layer bottom ($z_{invb}$)

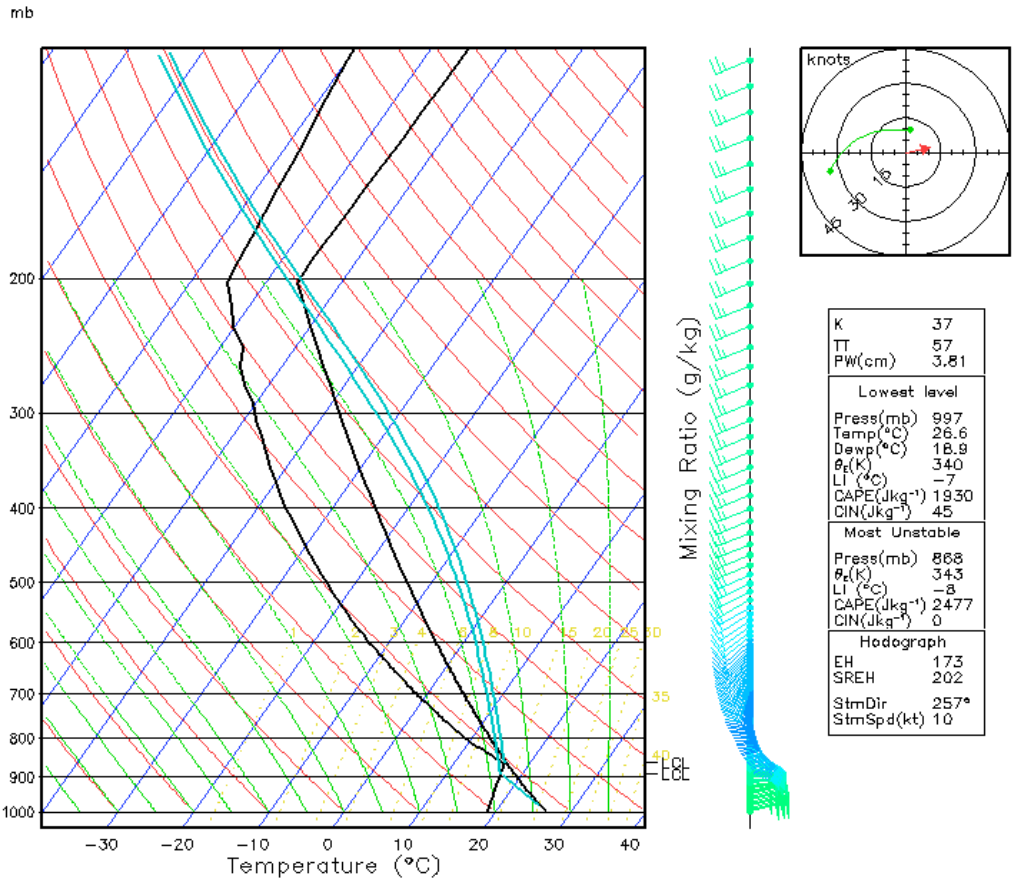


Figure 3.1: Sounding of the control simulation for 500-meter shear later depth and a low-level vertical shear magnitude of 7 m $s^{-1}$. The hodograph pictured in the top left corner only goes to 6 kilometers.

being set to 1250 meters.

Each sounding has a CAPE value of 2477 $J\ kg^{-1}$ with an LCL of around 950 mb. The LCL stays constant throughout all the simulations. An example of the thermodynamic profile can be seen in Figure 3.1.

### 3.2.2 Wind Profiles

In this study, the focus is being placed on the low-level wind profile below a variable depth ($d$), so for each simulation the deep-layer wind profile will remain

unchanged. A deep-layer hodograph supportive of supercells, consisting of a quarter-circle, clockwise turning, with unidirectional westerly shear above 2 km, will be used in each simulation run. With the deep-layer wind profile remaining unchanged, each simulation should have a relatively consistent storm motion and storm-relative winds. The equations below were adapted from Weisman and Klemp (1982) and show how the base state winds were calculated. These equations were modified for each simulation. $\Theta = 90(\frac{h}{u_{depth1}})(\frac{\pi}{180})$, $u_{max1}$ is the u-component of the wind at the bottom of the shear layer, $u_{max2}$ is the u-component of the wind at the top of the shear layer, $v_{max} = u_{max1}$, $u_{depth1}$ is the height of the top of the shear layer, $u_{depth2}$ is the height of the top the next layer, and $h$ is the height.

$$U(z) = \begin{cases} u_{max1} - [u_{max1} cos(\Theta)], & h < u_{depth1}. \\ u_{max1} + \frac{(h - u_{depth1})(u_{max2} - u_{max1})}{u_{depth2} - u_{depth1}}, & u_{depth1} \leq h < u_{depth2}. \\ u_{max2}, & h \geq u_{depth2}. \end{cases} \tag{3.3}$$

$$V(z) = \begin{cases} v_{max} sin(\Theta), & h < u_{depth1}. \\ v_{max}, & u_{depth1} \leq h < u_{depth2}. \\ v_{max}, & h \geq u_{depth2}. \end{cases} \tag{3.4}$$

The simulations in this study are categorized by their low-level wind shear orientation, low-level wind shear magnitude, and low-level shear layer depth. Three low-level shear layer depths will be tested in this experiment: 250-meters, 500-meters,

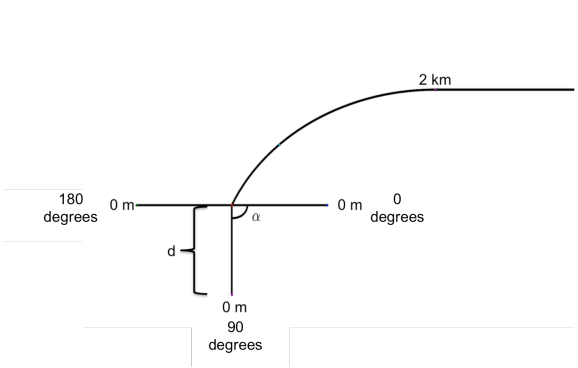


Figure 3.2: Modifications to hodograph.

and 1 kilometer. For each depth, a control simulation is first conducted in which the winds in the shear layer are held constant (i.e., shear magnitude of zero). The remaining experiments then involve adding shear layers oriented at 0° (easterly shear), 90° (southerly shear), or 180° (westerly shear), as illustrated in Fig. 1. All cases are carried out with a shear magnitude of 7 m $s^{-1}$, while the cases with 500 m depth are then repeated with a magnitude of 15 m $s^{-1}$. Table 3.2 below shows each simulation run and how it will be referred to when comparisons are made.

The changing orientation of the low-level shear will affect the gust-front relative winds, with the anticipated effect of causing the outflow boundary of each storm to lie in different positions. In the 180° case the environmental gust-front relative winds will be the strongest, whereas they are weakest in the 0°case. How the orientation of the low-level shear affects the gust front relative winds and gust front normal shear is expected to be very important in the supercell simulations.

One factor that must be taken into account is the storm-relative environmental helicity (SREH). The SREH is a measure of the streamwise vorticity within the

Table 3.2: Simulation run names

| **7 m s$^{-1}$** | **Control** | **0 Degrees** | **90 Degrees** | **180 Degrees** |
|---|---|---|---|---|
| **250 meter** | CTL-250M-7MS | 0DEG-250M-7MS | 90DEG-250M-7MS | 180DEG-250M-7MS |
| **500 meter** | CTL-500M-7MS | 0DEG-500M-7MS | 90DEG-500M-7MS | 180DEG-500M-7MS |
| **1 kilometer** | CTL-1KM-7MS | 0DEG-1KM-7MS | 90DEG-1KM-7MS | 180DEG-1KM-7MS |

| **15 m s$^{-1}$** | | | | |
|---|---|---|---|---|
| **500 meter** | CTL-500M-15MS | 0DEG-500M-15MS | 90DEG-500M-15MS | 180DEG-500M-15MS |

inflow environment of a convective storm (Davies-Jones et al., 1990). As the SREH increases, so too does the possibility that a supercell will become tornadic (e.g., Craven and Brooks 2004). In order to isolate the role of low-level shear on only cold pool propagation, the SREH should be kept consistent between all runs. Unfortunately, this is difficult to accomplish because the orientation of the low-level winds, in part determines, SREH. How these values change is shown in Table 3.3. The SREH here is calculated through a depth of 0-3 km.

Table 3.3: SREH Values, calculated over a 0-3 km depth, for each simulation run.

| SREH ($m^2 s^{-2}$) | Control Simulations | 0° Simulations | 90° Simulations | 180° Simulations |
|---|---|---|---|---|
| 250 meter Shear Layer | 260 | 286 | 338 | 234 |
| 500 meter Shear Layer | 202 | 228 | 323 | 175 |
| 1 kilometer Shear Layer | 109 | 113 | 226 | 106 |

# 4 RESULTS AND DISCUSSION

In this section, the results of each simulation run are shown and discussed. The 500-meter shear layer, weak shear (7 m $s^{-1}$) cases are described first. It will be followed by two simulations, one that decreases (250-m) and one that increases (1 km) the shear layer depth. Finally, simulations which increase (15 m $s^{-1}$) the wind shear magnitude for the 500-meter shear layer cases will be described. How each of the parameter changes affects the emerging trends will be discussed.

Each simulation was initialized by a warm bubble and a storm begins to develop around 2100 seconds (35 minutes). Almost as soon as the storms begin each simulation takes on its own look and features. Supercell characteristics begin to appear around 3000 seconds (50 minutes).

## 4.1 Influence of Shear Vector Orientation

Figure 4.1 shows the simulated reflectivity of each simulation at the time of maximum surface vertical vorticity at the lowest grid level. 0DEG-500M-7MS has its maximum at the earliest time of 7800 seconds (130 minutes), with 90DEG-500M-7MS following at 9900 seconds (165 minutes). Both CTL-500M-7MS and 180DEG-500M-7MS have their maximum vertical vorticity at the very end of the simulation (180 minutes).

In these figures the midlevel mesocyclone is located using the midlevel (4 km)

vertical velocity plotted every 5 m $s^{-1}$. In both CTL-500M-7MS and 180DEG-500M-7MS, the outflow is restrained behind (i.e., west of) the midlevel mesocyclone. In 0DEG-500M-7MS the outflow is aligned with the south-eastern edge of the midlevel mesocyclone, positioning it right below. The maximum near-ground vertical vorticity also occurs earliest in 0DEG-500M-7MS, possibly due to the alignment of the outflow relative to the midlevel mesocyclone.

Another big difference between 0DEG-500M-7MS and the other 500-meter simulations is the updraft shape. In 0DEG-500M-7MS the updraft is curved around the hook echo, while in the other simulations a hook echo does not even appear to exist and the updraft is more circular.

There are also significant differences in the reflectivity structure of each storm as well as the orientation of the gust front. Both CTL-500M-7MS and 180DEG-500M-7MS have gust fronts oriented west to east with an elongated reflectivity structure. In contrast, 0DEG-500M-7MS and 90DEG-500M-7MS have gust front relative winds oriented in a more south to north pattern. 0DEG-500M-7MS also appears to be rain-wrapped and is the only simulation with the surface vertical vorticity max positioned beneath the midlevel mesocyclone during the time of maximum surface vertical vorticity.

Surface circulation was plotted in order to analyze how the changing orientation of low-level wind shear was affecting the near-ground rotation. Circulation for each run was calculated by averaging the surface vertical vorticity about a 2-km square

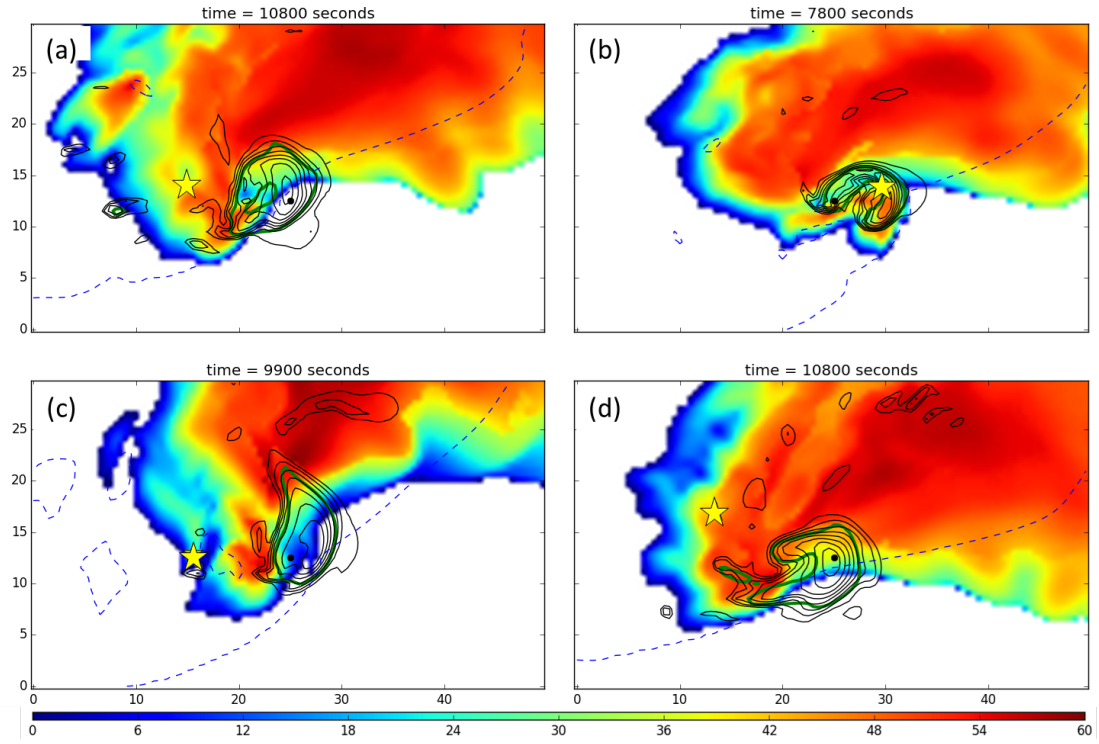


Figure 4.1: Simulated surface reflectivity (shaded) for **(a)** CTL-500M-7MS, **(b)** 0DEG-500M-7MS, **(c)** 90DEG-500M-7MS, and **(d)** 180DEG-500M-7MS at the time of maximum vertical vorticity at the lowest grid level. The dashed blue line is the -1 K potential temperature contour at the surface, black contours are mid-level (4 km) vertical velocity plotted every 5 m $s^{-1}$, solid green line is the 600 $m^2s^{-2}$ updraft helicity outline (integrated 1-6 km), black dot is the maximum updraft helicity (integrated 1-6 km), and the yellow star is the maximum near-ground (surface) vertical vorticity. The x and y-axis are in km and the colorbar is DBZ.

centered on each grid point (Eq. 4.1). This equation shows that circulation is just the integral over an area of vertical vorticity. Circulation, then, can be though of as the average vertical vorticity over a specific area. Plotting the surface circulation allows for a broader view of the surface rotation. Vertical vorticity gives a more instant view of rotation for a single point where circulation looks more at how the surrounding rotation interacts with itself.

$$\Gamma = \int_A \zeta \, dA \tag{4.1}$$

Figure 4.2 shows the near-ground circulation for the same time as the reflectivity for each simulation. There appears to be a large difference in not only the strength of the circulation, but also the positioning of the maximum. 0DEG-500M-7MS has increased near-ground rotation, with a large amount of cyclonic rotation (i.e. positive circulation) below the midlevel mesocyclone, while the other cases appear to have the circulation constrained behind the midlevel mesocyclone. 0DEG-500M-7MS also has a positive/negative cirulation couplet which is consistent with vortex line arch discussed in Markowski et al. (2008). The circulation in 180DEG-500M-7MS is constrained behind the midlevel mesocyclone while in 90DEG-500M-7MS and CTL-500M-7MS it is also constrained, but much less. The 90DEG-500M-7MS does have increased circulation underneath the midlevel mesocyclone, but this does not occur until the end of the simulation (not shown).

Figure 4.3(a-d) is a time series of the change in distance between the maximum near-ground rotation and the midlevel mesocyclone. The distance calculations were

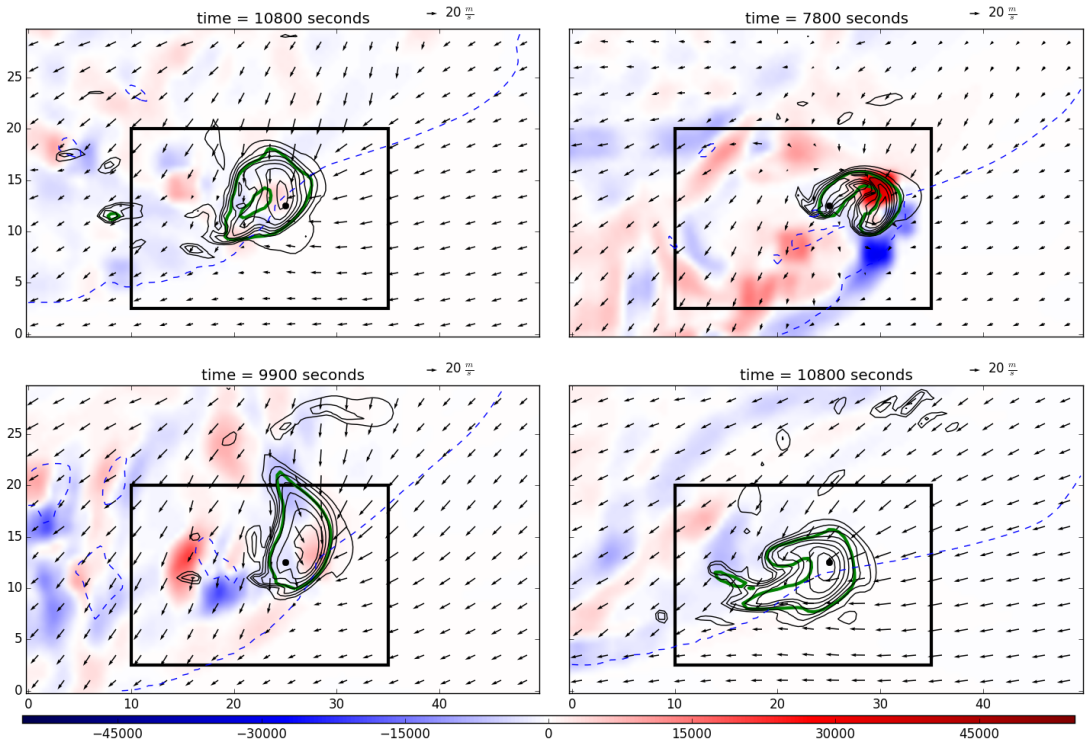


Figure 4.2: Surface circulation computed about a 2-km square centered on each grid point for **(a)** CTL-500M-7MS, **(b)** 0DEG-500M-7MS, **(c)** 90DEG-500M-7MS, and **(d)** 180DEG-500M-7MS at the time of maximum vertical vorticity at the lowest grid level. The black contours are mid-level (4 km) vertical velocity plotted every 5 m $s^{-1}$, solid green line is the 600 $m^2s^{-2}$ updraft helicity outline (integrated 1-6 km), black dot is the maximum updraft helicity (integrated 1-6 km), and the yellow star is the maximum near-ground (surface) vertical vorticity. The arrows are the u and v-component of the surface winds. The black box represents the area in which subsequent distance calculations were performed. The black box is determined by the position of the maximum updraft helicity having dimensions of 25 x 17.5 km. The x and y-axis are in km and the colorbar is $m^2s^{-1}$.

performed in a rectangular area having dimensions of 25 x 17.5 km determined by the maximum updraft helicity; this keeps the calculations focused on the area of the storm important to this study: the area around the midlevel mesocyclone. This is because the study focuses on the position of the outflow relative to the midlevel mesocyclone, and if the region is not specified the distance calculations could pick up on other areas of the storm. Figure 4.2 shows this area. The distance equation (Eq. 4.2) was used for the calculations, using the grid points of the maximum near-ground circulation ($x_1$,$y_1$) and the maximum updraft helicity ($x_2$,$y_2$).

$$D = \sqrt{(x_2 - x_1)^2 + (y_2 - y_1)^2} \tag{4.2}$$

Figure 4.3(a-d) shows not only the distance between the circulation and the midlevel mesocyclone, but it also shows where the midlevel mesocyclone is in relation to the maximum near-ground circulation. The positive distances correspond to the midlevel mesocyclone being located ahead of the near-ground circulation, while the negative values correspond to a location behind the near-ground circulation.

$$UH = -\int_0^6 \zeta \cdot w \, dz \tag{4.3}$$

In the same figure, there is also a time series of the maximum near-ground vertical vorticity and updraft helicity, which is integrated over a 0-6 km layer. Updraft helicity is defined as the how the vertical vorticity interacts with the vertical winds within a certain depth (Eq. 4.3, Weisman and Rotunno 2000). In each case, with the

exception of the end of 90DEG-500M-7MS, the updraft helicity remains relatively consistent throughout the run. While it is not possible to completely negate the effects of dynamic forcing, this hopefully will keep it consistent enough to assume that the largest affect is coming from the positioning of the dynamic forcing. When run for an hour longer (not shown), 90DEG-500M-7MS did show an increase in updraft helicity as the distance between the midlevel mesocyclone and the near-ground circulation decreased, but leveled back out after approximately 30 minutes. Figure 4.3(e) shows the maximum near-ground circulation.

The results seen in Figure 4.3 agree with findings from the previous two figures. It is clear 0DEG-500M-7MS has the strongest maximum circulation (red line, Fig. 4.3e), corresponding to the time of an increase in low-level vertical vorticity. At the time of increase for both of these parameters, the distance between the near-ground circulation and the midlevel mesocyclone also begins to shrink (Fig. 4.3b). 90DEG-500M-7MS had the second highest maximum circulation, although it does not appear until the end of the run. Like 0DEG-500M-7MS, this rise in maximum circulation corresponds to a decrease in the distance, and it is at that time (8400 sec) that the updraft helicity and vertical vorticity begin to increase in intensity.

In CTL-500M-7MS and 180DEG-500M-7MS the distance between the near-ground circulation and the midlevel mesocyclone remains large, with only slight fluctuations, and so the low-level vertical vorticity remains weak and unchanging and the circulation is correspondingly low. 90DEG-500M-7MS was run for an hour

longer (not shown) under suspicion that it would eventually end up looking similar to 0DEG-500M-7MS. Results of that simulation showed that around 185 minutes (just over 3 hours) the distance in the 90 degree case drops, and an increase in the circulation and low-level vertical vorticity can be seen, much like 0DEG-500M-7MS. The circulation maximum peaks at 40000 $m^2$ $s^{-2}$ around 12,300 seconds ( 3 hours and 25 minutes) which corresponds with a spike in the maximum surface vertical vorticity (0.09 $s^{-1}$) and a 10,200-meter drop in distance.

### 4.1.1 Discussion

The orientation of the low-level shear vector and the gust front relative winds do appear to affect the positioning of the midlevel mesocyclone relative to the outflow in simulated supercells. 0DEG-500M-7MS, which aligns the midlevel mesocyclone with the leading edge of the outflow, appears to have the most favorable conditions for enhanced near-ground rotation. 90DEG-500M-7MS comes close to replicating 0DEG-500M-7MS but must be simulated an hour longer before similarities are seen. The low-level storm-relative winds in this case opposes the gust front, more so that 0DEG-500M-7MS, so it takes the outflow longer to get positioned below the midlevel mesocyclone.

There appears to be a connection between the distance and the near-ground rotation. Surface vertical vorticity was generally strongest when the distance between the midlevel mesocyclone and the maximum surface circulation was relatively small. In these simulations, a low-level shear orientation of 0° relative to the deep-layer

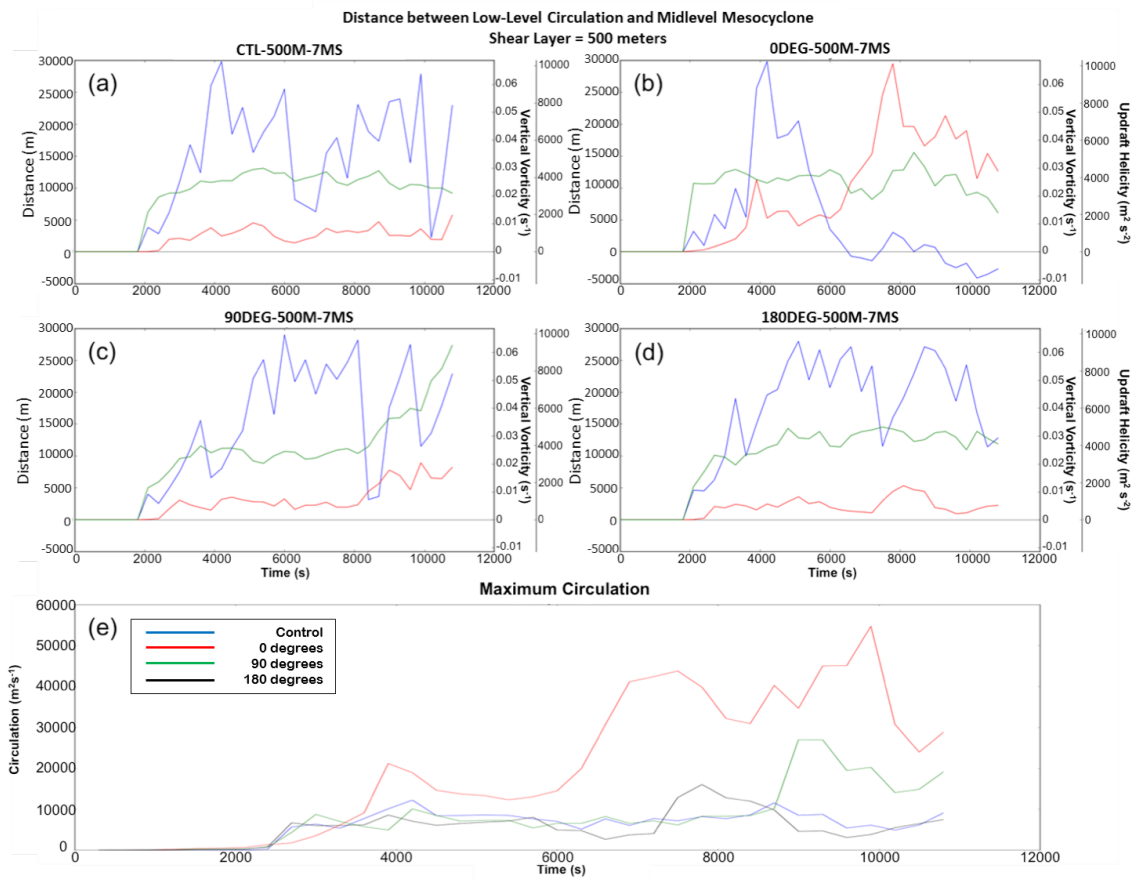


Figure 4.3: 500-meter shear layer depth **(a) - (d):** time series of the distance between the maximum updraft helicity and the maximum low-level circulation (blue lines), the maximum surface vertical vorticity (red lines), the maximum 1-6 km updraft helicity (green lines). **(e):** Time series of the maximum circulation for CTL-500M-7MS (blue), 0DEG-500M-7MS (red), 90DEG-500M-7MS (green), and 180DEG-500M-7MS (black).

wind profile leads to the smallest distance between the midlevel mesocyclone and maximum low-level circulation, resulting in the strongest vertical vorticity near the surface. In CTL-500M-7MS and 180DEG-500M-7MS the distance remains large as the orientation of the low-level vertical wind shear and the gust front relative winds position the outflow too far behind the midlevel mesocyclone to develop appreciable near-ground rotation.

## 4.2 Influence of the Shear-Layer Depth

With promising results seen in the 500-meter shear layer runs, the next step was to change the depth of the shear layer. The question here is: how does the depth of the shear layer affect the sensitivity of the storms to shear orientation? In other words, how does the depth affect the trends seen in the previous section?

Figure 4.4 shows similar reflectivity plots to those in Figure 4.1, with the reflectivity still being shown at the time of maximum low-level vertical vorticity for each simulation run. The 250-meter shear layer run is shown on the left, the 500-meter run in the middle, and the 1 kilometer shear layer run is shown on the right. Similarly, Figure 4.5 shows the circulation.

The 250-meter shear layer case shows similar results to the 500-meter case. 0DEG-250M-7MS is aligned with the outflow boundary, and cyclonic circulation develops right below the midlevel mesocyclone, just like 0DEG-500M-7MS. Again, in 180DEG-250M-7MS the outflow is restrained behind the midlevel mesocyclone and the circulation is weak and develops mostly behind the storm. In CTL-250M-7MS and 90DEG-250M-7MS, however, there is some outflow underneath the midlevel mesocyclone, but the circulation is still weak.

The only major differences between the 500-meter case and the 250-meter case is the time of maximum surface vertical vorticity. CTL-250M-7MS, 90DEG-250M-7MS, and 180DEG-250M-7MS all have their maximum occur before their 500-meter counterparts. 0DEG-250M-7MS occurs last, right at the end of the simulation. An-

other slight difference in these runs is the positioning of the maximum surface vertical vorticity, which is not within each of the midlevel mesocyclones, with an exception of the 180DEG-250M-7MS run.

The distances and circulation intensity (Fig. 4.6) also show similar results to the 500-meter case. 0DEG-250M-7MS has the smallest distance and the strongest near-ground circulation. What is interesting here, when compared to 0DEG-500M-7MS, is that while the distance is small, it is never negative; the midlevel mesocyclone is never out ahead of the maximum near-ground circulation. Finally, the other three cases all have relatively large distances and low maximum near-ground circulation. This is different from 90DEG-500M-7MS which begins to spike at the end of the simulation. Here, there is a small spike, but nothing as notable as what has been seen in the previous runs.

In the 1 kilometer case, differences are much more apparent when compared to the previous two cases. Increasing the shear layer depth to 1 kilometer seems to have made a difference in the positioning of the outflow relative to the overlying midlevel mesocyclone. 0DEG-1KM-7MS now has the outflow surging ahead unlike in 0DEG-500M-7MS which had the outflow aligned with the eastern edge of the midlevel mesocyclone. CTL-1KM-7MS and 90DEG-1KM-7MS appear to have the outflow lined up with the south-eastern edge of the midlevel mesocyclone, while in 180DEG-1KM-7MS the outflow is still slightly restrained.

This result shows up well in the circulation plots, where CTL-1KM-7MS and

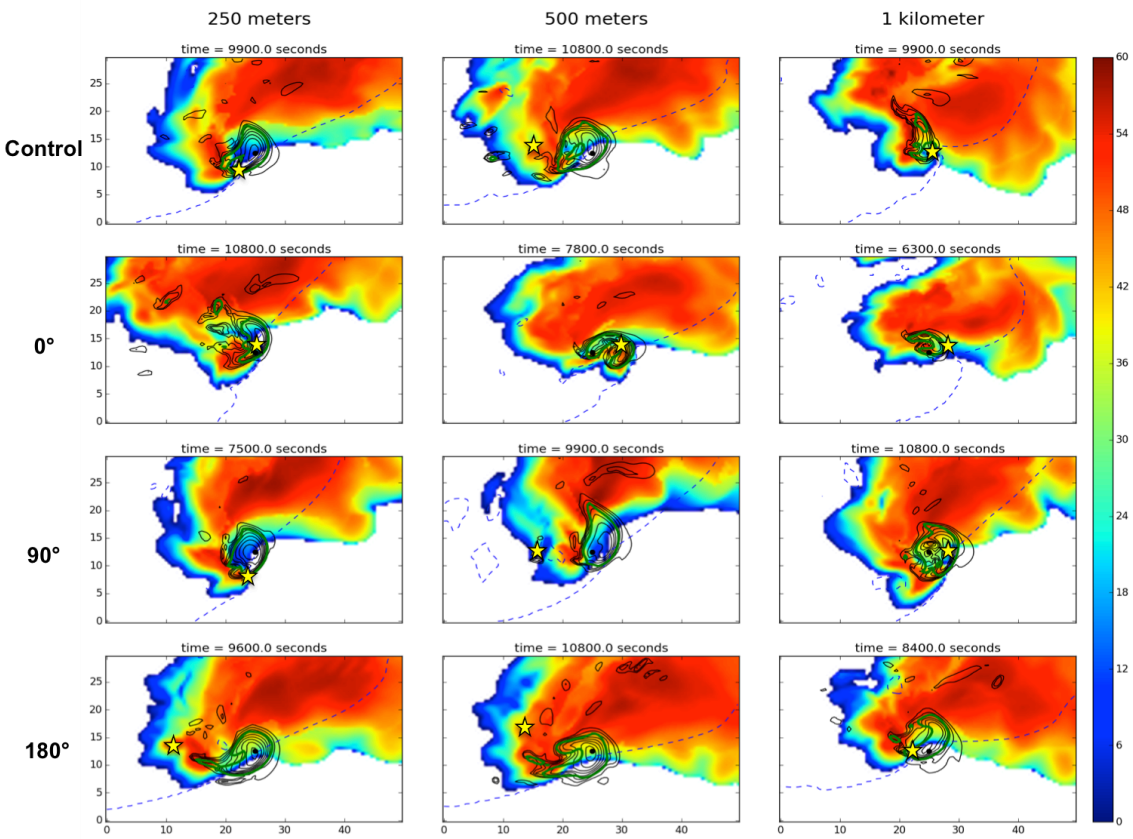


Figure 4.4: Similar to Figure 4.1 but for the 250-meter, 500-meter, and 1 kilometer simulations.

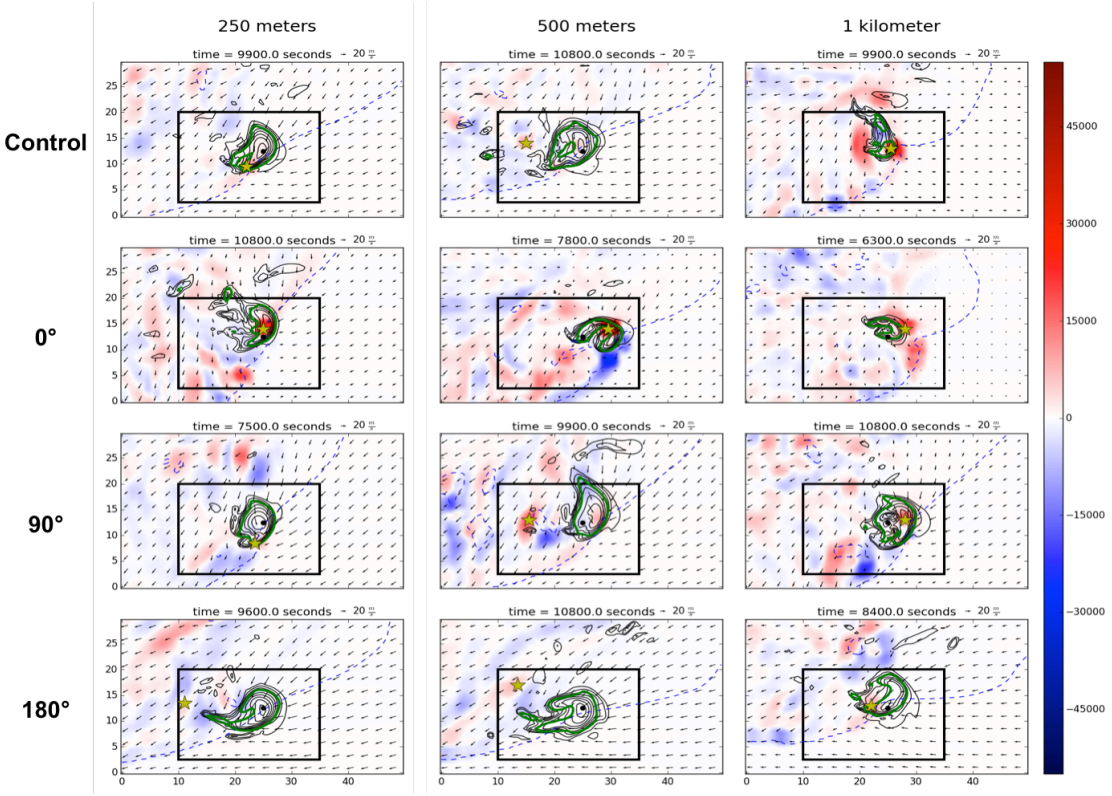


Figure 4.5: Similar to Figure 4.2 but for the 250-meter, 500-meter, and 1 kilometer simulations.

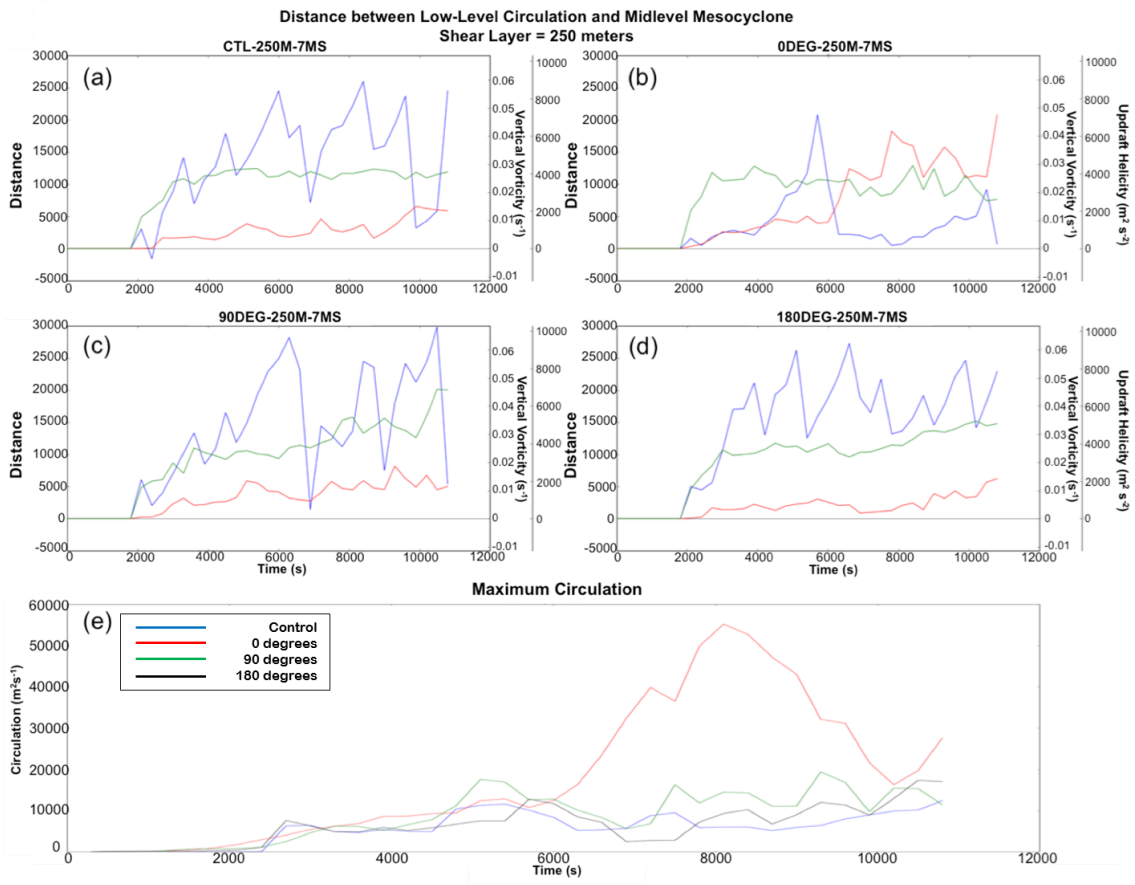


Figure 4.6: Same as figure 4.3 but for the 250-meter shear layer depth case.

90DEG-1KM-7MS are now seen with stronger circulation and the positioning below the midlevel mesocyclone. Looking at the distances for these storm simulations (Fig. 4.7), we now see that the distance between the maximum circulation and the midlevel mesocyclone has increased for 0DEG-1KM-7MS, but the near-ground circulation has also surged out ahead. CTL-1KM-7MS now ends up with the smallest distance and a greater near-ground circulation. In 180DEG-1KM-7MS there are two spikes where the distance drops dramatically but there is not a spike in surface vertical vorticity. This is because most of the outflow is still restrained behind the storm, so the increase in vertical vorticity happens outside of the area where calculations are performed.

### 4.2.1 Discussion

While there are some differences between each shear layer depth, there is still an effect seen from the changing orientation of the low-level wind shear. The 250-meter cases are similar to the 500-meter cases, although with a smaller shear layer depth the effects are more subdued. The 1 kilometer cases on the other hand, have enhanced the effects of the low-level shear orientation. Where once the 0° case was the most favorable scenario, here the shear and gust front relative winds are weaker over a greater depth and this allows the outflow to surge far out ahead of the midlevel mesocyclone, causing large distances and a decreased maximum surface circulation. CTL-1KM-7MS is the most favorable case for the 1 kilometer shear later depth in terms of outflow positioning.

The orientation still has an effect on the position of the midlevel mesocyclone

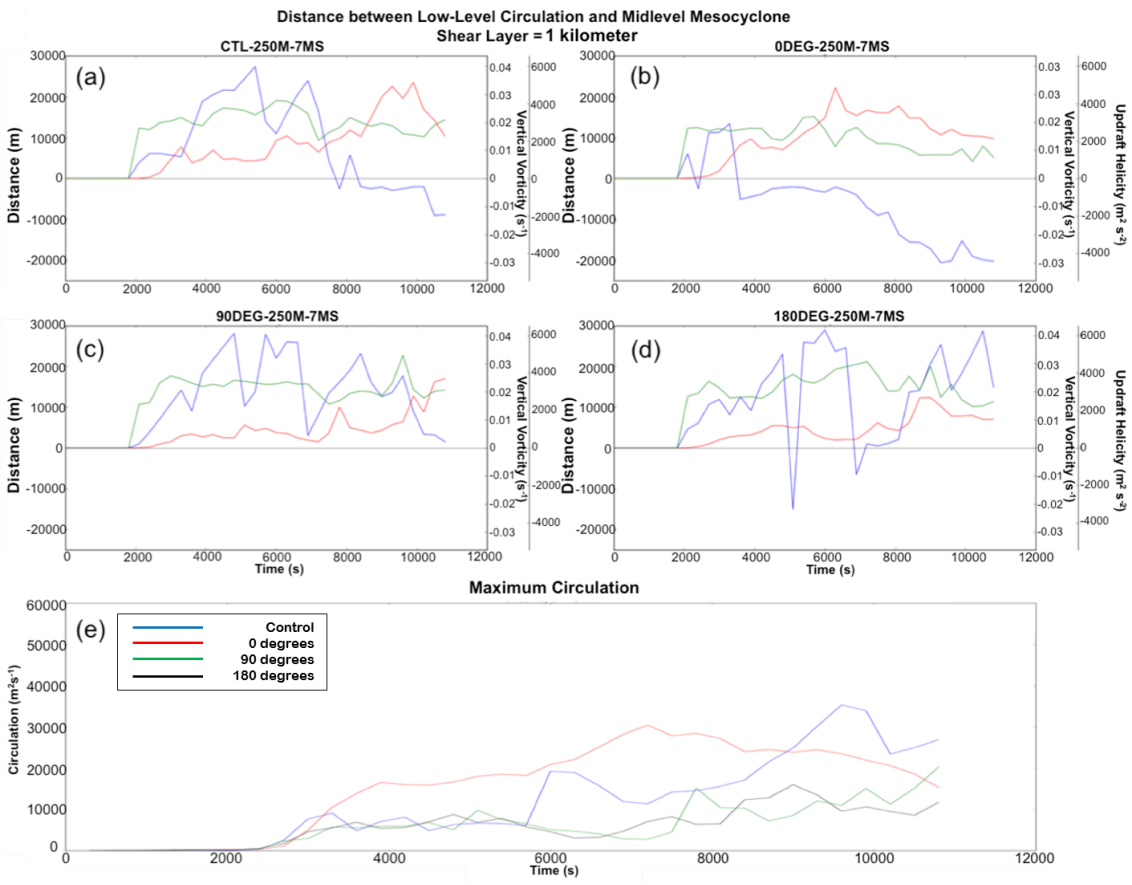


Figure 4.7: Same as figure 4.3 but for the 1 kilometer shear layer depth case.

with respect to the outflow, but when the shear depth is increased to 1 kilometer, the most favorable simulation changes. However, all the other trends remain the same, with the surface vertical vorticity still being strongest when the distance is small. A last point that is interesting to note is that even though it is less dramatic, the 250-meter cases still affect the simulated storms, leading to a question of how small does the shear depth need to be before differences are no longer seen?

One last interesting note is for both the 500-meter and 250-meter shear layer depth simulations, the SREH is less in the 0° cases than in the 90° cases, and yet the 0° has the stronger near-ground rotation. Despite the less favorable SREH in the 0° case, the shear orientation/distance effect seems to triumph over it.

### 4.3 Statistical Comparison

Combining all the data from the previous three runs (500-meter, 250-meter, and 1 kilometer shear layers) we can look at statistics on the distances between the maximum near-ground circulation and the midlevel mesocyclone. These calculations are at 5 minute increments and remove the first hour of data because the storm is either still developing or non-existent.

Figure 4.8 looks at the correlation between the distance and two different parameters, the low-level vertical vorticity and the near-ground circulation. If there is a p-value of less than 0.01 a correlation is considered statistically significant. This value means the there is less then 1% of a chance that the correlation seen is completely

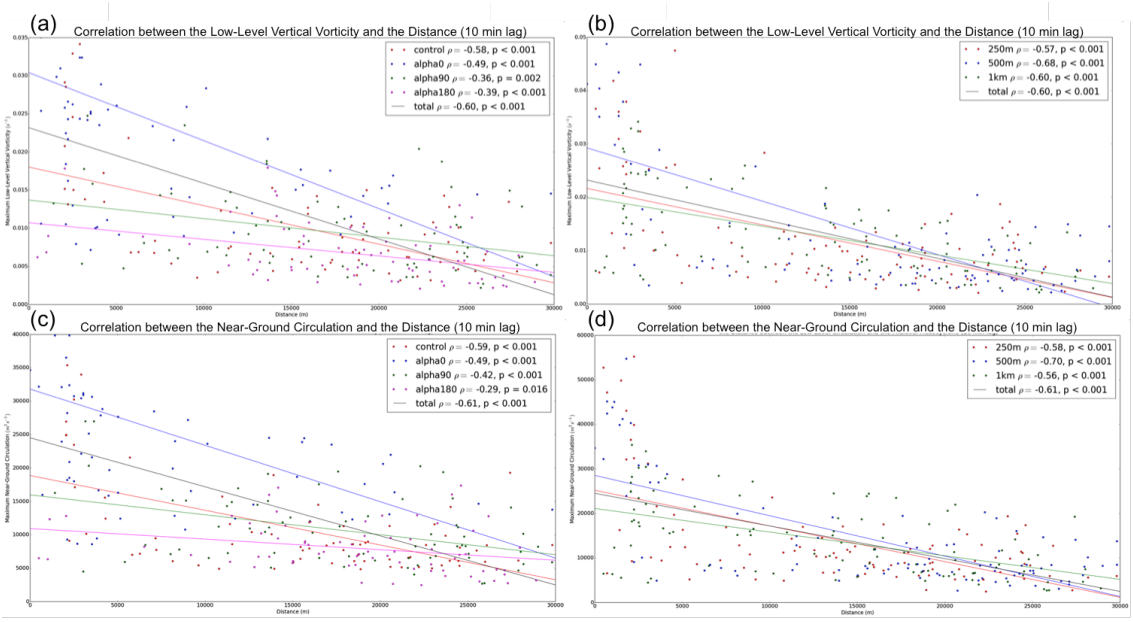


Figure 4.8: **(a):** Correlation between distance and maximum low-level vertical vorticity with a 10 minute lag, separated by critical angle. **(b):** Correlation between distance and low-level vertical vorticity with a 10 minute lag, separated by shear layer depth. **(c):** Correlation between Distance and near-ground circulation with a 10 minute lag, separated by critical angle. **(d):** Correlation between Distance and near-ground circulation with a 10 minute lag, separated by shear layer depth.

by chance. There is a statistically significant negative correlation between either the near-ground maximum vertical vorticity or the circulation and the distance. When separated by critical angle, the strongest correlations can be seen in the control (no shear) case, while when separated by shear layer depth, the strongest correlations are in the 500-meter case. A time lag of 10 minutes has been implemented in the plots on the maximum vertical vorticity and the maximum near-ground circulation because the distance may not influence the parameters instantaneously. Multiple time lags were tested and the 10 minute lag was found to have the strongest correlations.

Looking at box-and-whiskers plots (Fig. 4.9(a-b)) it is more clear that the

critical angles are having an effect on distances. The 0 degree case has the lowest distances out off all the shear orientations. When looking between shear layer depths there is not much differences in the median values, but the range of values does increase as the shear layer depth increases. Figures 4.9(c-e) show the different angles now separated into their different shear layer depths. It is interesting to note the contrast between the 0DEG-500M-7MS case and all the other critical angles in the same shear layer. This same pattern can be seen in the 250-meter shear layer case as well as the 1-kilometer case. The largest difference is seen in 0DEG-500M-7MS (4.9d) and 0DEG-1KM-7MS (4.9e), where, unlike 0DEG-250M-7MS (4.10c), the distances go negative. This is most likely because the magnitude of winds are spread over a larger layer, allowing the circulation-rich outflow to move out ahead of the midlevel mesocyclone. In 0DEG-250M-7MS the effects of the low-level shear is constrained to a smaller layer, which means the gust front does not advance as quickly as in the simulations with greated shear depths.

Figure 4.10 is similar to Figure 4.9 but it shows the maximum vertical vorticity at the surface. Looking at the separation of the maximum vertical vorticity separated by shear orientation (Figure 4.10a) the 0° cases have the largest maximum surface vertical vorticity. When looking at each case separated out (Figure 4.10c-e) the trend is seen for 250 meters and 500 meters, with 1 kilometer showing less of the same trend.

Finally, Figure 4.11 show box-and-whisker plots of the average surface circu-

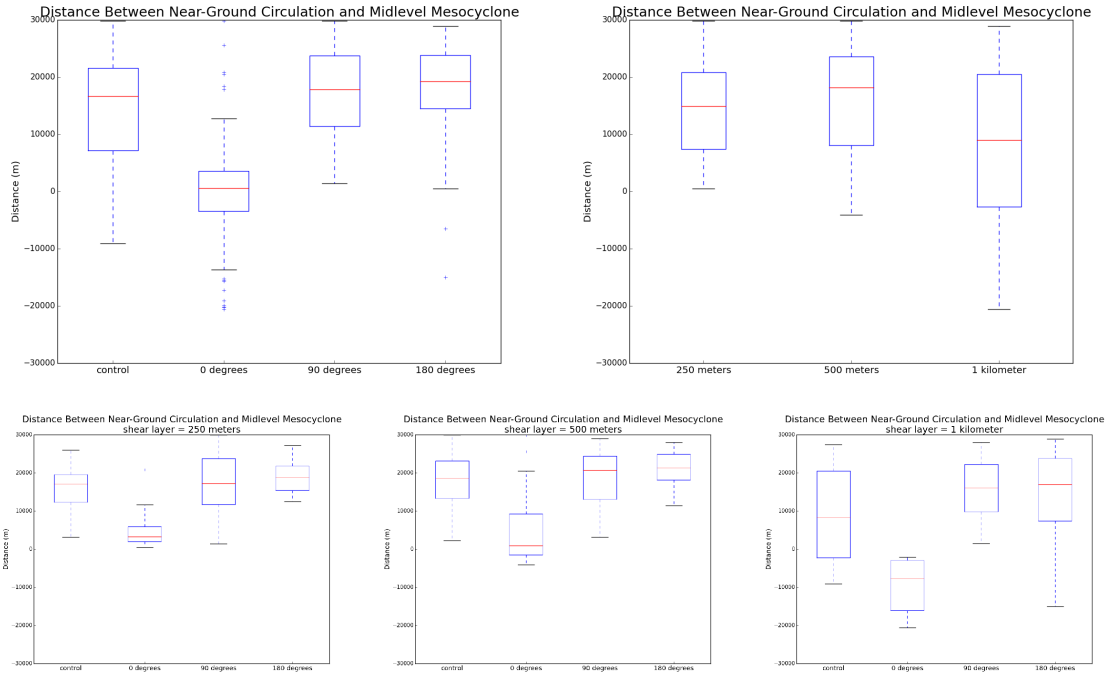


Figure 4.9: **(a):** Box and whiskers plot of the distance between the low-level circulation and midlevel mesocyclone categorized by angle. **(b):** Box and whiskers plot of the distance between the low-level circulation and midlevel mesocyclone categorized by shear layer. **(c)-(e):** Box and whiskers plots as above, split into each of the three shear layers categorized by angle.

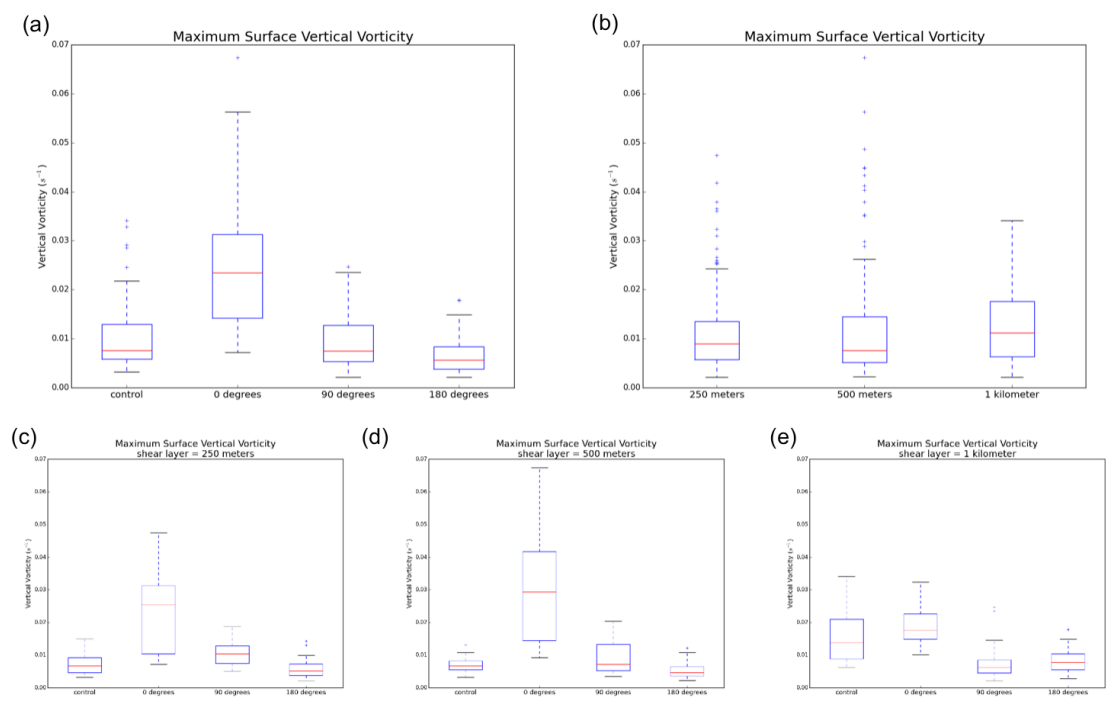


Figure 4.10: Similar to figure 4.9, but for maximum vertical vorticity.

lation below and within a 500 $m^2s^{-2}$ updraft helicity contour. This shows us the average circulation below the updraft in the midlevel mesocyclone, thus, it shows for each simulation, a rough measure of the vorticity available to be stretched/converged. Once again, the 0° cases have the largest average surface circulation, with the exception of the 1 kilometer shear depth.

### 4.3.1 Discussion

The statistical comparisons shown herein support the hypotheses put forth at the beginning of this study. This analysis supports the hypothesis that the orientation of the shear vector affects the distance between the midlevel mesocyclone and the near-ground rotation. There is a statistically significant correlation seen between

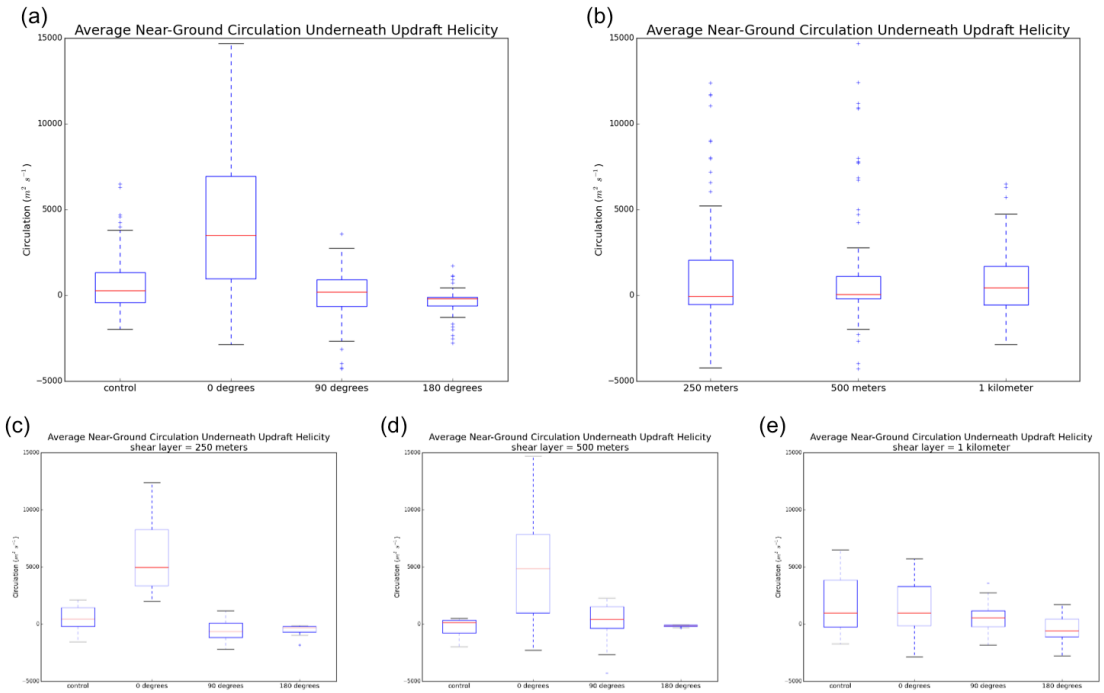


Figure 4.11: Similar to figure 4.9, but for average surface circulation below a 500 $m^2s^{-2}$ updraft helicity contour.

the midlevel mesocyclone/maximum near-ground circulation distance and both the maximum surface circulation and the maximum low-level vertical vorticity.

The box-and-whisker plots also support the results in the previous two sections. Both 0DEG-500M-7MS and 0DEG-250M-7MS have the smallest distances corresponding with the strongest maximum surface vertical vorticity and near-ground circulation. 0DEG-1KM-7MS does have lower distances than the other cases, but its magnitude is larger than the other shear orientations. Looking at both Figure 4.10 and 4.11, 0DEG-500M-7MS and 0DEG-250M-7MS have a wider range of values than the other angles. This is possible because of the outflow positioning below the midlevel mesocyclone. As the distance between the near-ground rotation and midlevel mesocyclone decrease, the surface vertical vorticity increases.

In the 1 kilometer case, the differences between the angles becomes much smaller than the other shear layer depth. Here, because of the depth of the shear layer, the 0DEG-1KM-7MS outflow surged ahead and the same thing happened with 90DEG-1KM-7MS. CTL-1KM-7MS and 180DEG-1KM-7MS did not have values close to 0° or 90° to begin with and now they are stronger because the outflow is getting closer to the midlevel mesocyclone, but the position may not yet be favorable to get the values seen in 0DEG-250M-7MS and 0DEG-500M-7MS.

## 4.4 Influence of Shear Magnitude

Another question to answer is how changing low-level shear magnitude affects each storm. These simulations use the 500-meter shear layer depth case, but the magnitude of the low-level vertical wind shear was intensified to 15 m $s^{-1}$.

In these simulations, the differences are much larger because of the significant increase in low-level vertical wind shear magnitude. The outflow in 0DEG-500M-15MS has surged ahead of the storm, effectively cutting off its inflow and causing the simulated storm to break down (Figure 4.12). This circumstance also causes the time of maximum surface vertical vorticity to occur very early in the storm's life cycle. In 90DEG-500M-15MS and 180DEG-500M-15MS, the outflow is restrained behind the midlevel mesocyclone. In 180DEG-500M-15MS, the storm takes on a kind of oblong shape.

Looking at the circulation (Figure 4.13) and the time series (Figure 4.14) for these simulations, it is clear that none of the storms are able to intensify much, if at all; the magnitude of the shear is keeping the storms from developing fully. The increase in magnitude is changing the storms much like the 1 kilometer shear layer depth. There is virtually no circulation below the midlevel mesocyclone and large distances between the midlevel mesocyclone and the maximum near-ground circulation. 0DEG-500M-15MS does have the strongest circulation, but it is nowhere near as large as the previous cases. The gust front relative winds are weak, allowing the outflow to surge ahead. In this same case the peak time of maximum surface

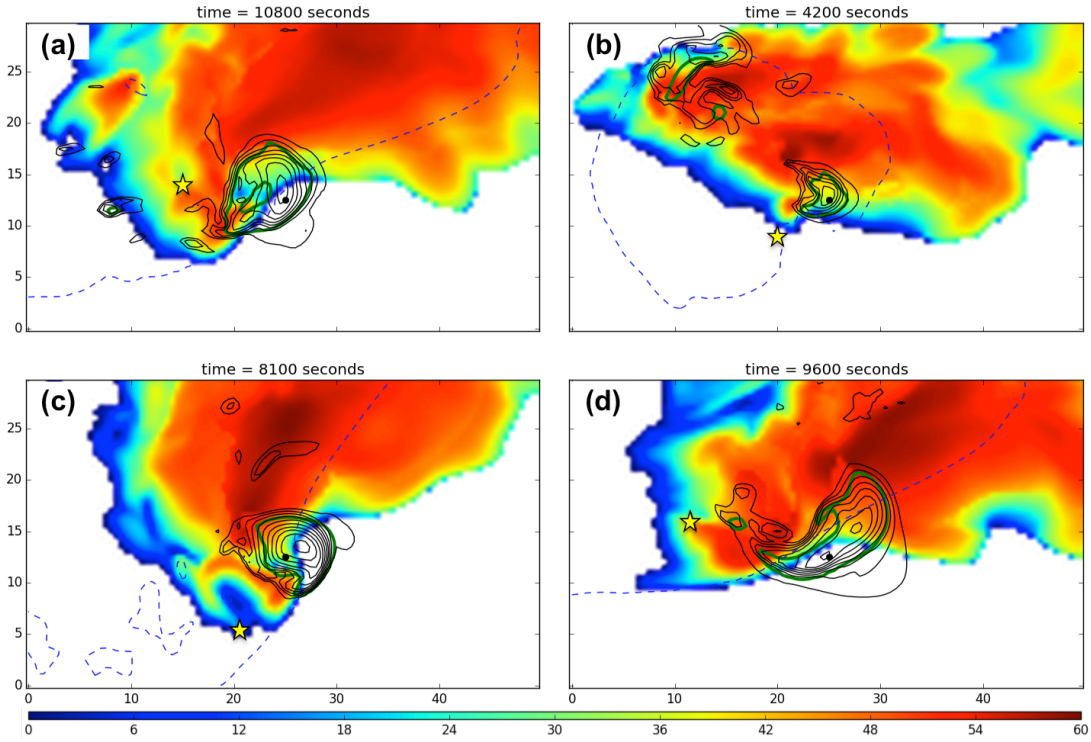


Figure 4.12: Same as 4.1, but for the 500-meter shear layer depth, 15 m $s^{-1}$ case.

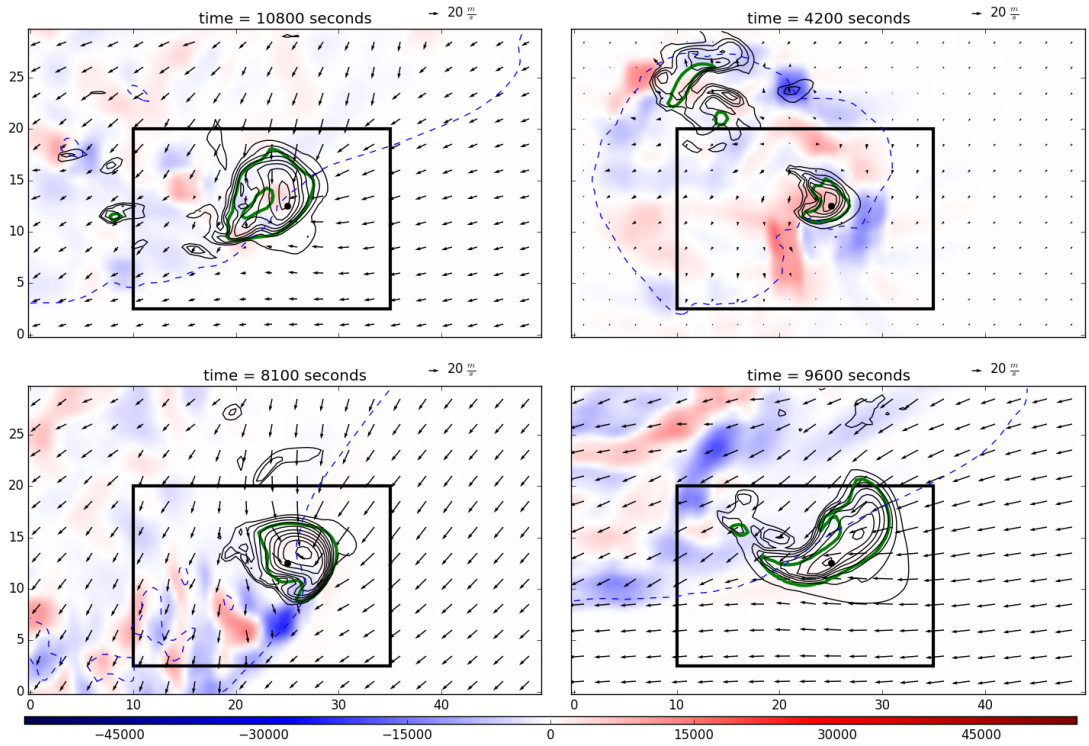


Figure 4.13: Same as 4.2, but for the 500-meter shear layer depth, 15 m $s^{-1}$ case.

vertical vorticity is very early at 4200 seconds ( 72 minutes). This is most likely because the storm dies early on from the large magnitude low-level shear.

### 4.4.1 Discussion

From the results seen above it seems as if the angle trends relative to the gust front/outflow are more amplified when the magnitude increases. They are so amplified that none of the cases are ideal for a tornadic supercell. The distances seen in each are too great, causing low surface circulation magnitudes, or sometimes a lack thereof, below the midlevel mesocyclone. With the amplitude of the low-level shear risen to 15 m $s^{-1}$, the orientation of the shear has a large effect on the gust front. In 0DEG-500M-15MS, the shear greatly over powers the gust front relative winds

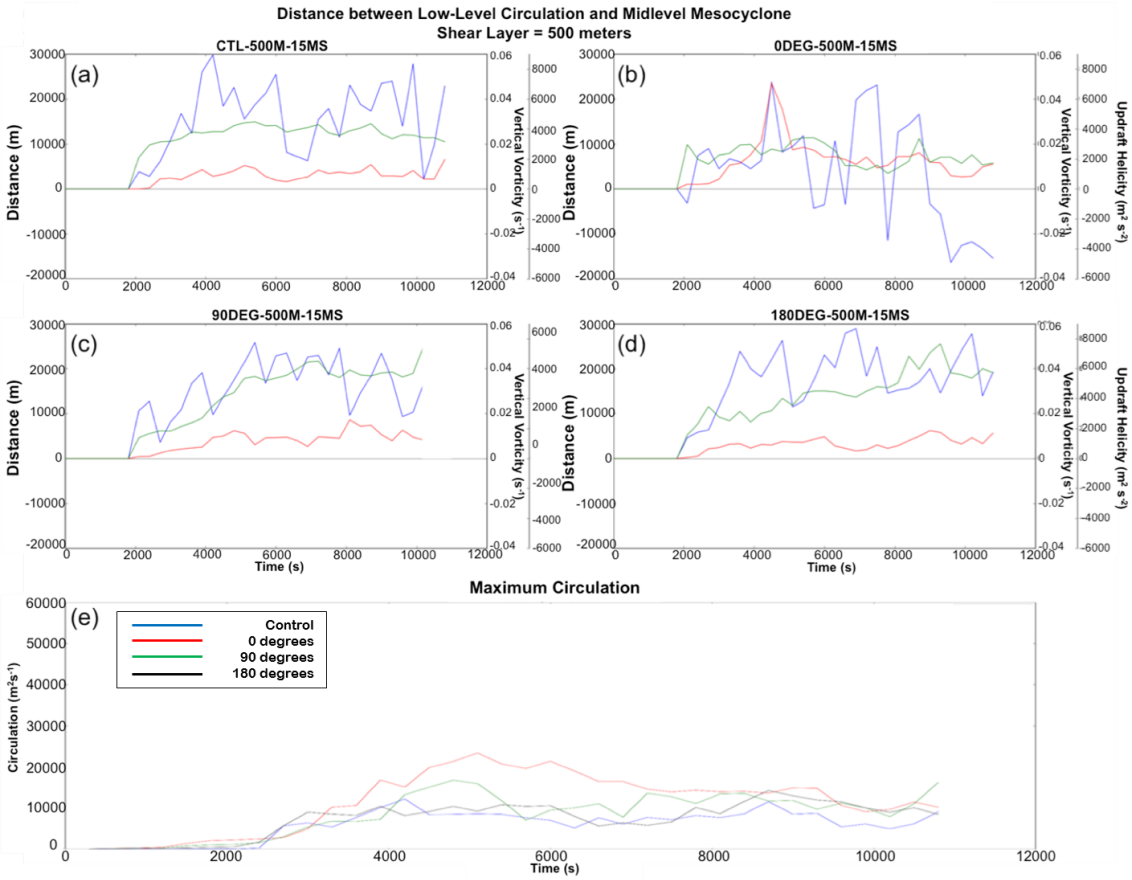


Figure 4.14: Same as figure 4.3 but for the 500-meter shear layer depth, 15 m $s^{-1}$ case.

and so the outflow surges ahead greatly, whereas 180DEG-500M-15MS amplifies the winds so much that the outflow is left way behind the storm. This cuts off the energy source of the simulated supercells, effectively causing an early dissipation.

It would be interesting to do another set of simulation runs with the 500-meter shear layer but changing the magnitude to 4 m $s^{-1}$. Would this lead to something similar to the 250-meter cases?

## 4.5 Cold Pool Intensity

As stated in Chapter 1, wind shear and cold pool interactions may have significant impacts on the existing supercell. So the question is here: are the distances driven by changes in the cold pool intensity or the ambient wind profile over the depth of the cold pool? Figure 4.15 shows the cold pool intensity (Eq. 4.4) for 12 simulation runs: three shear layer depths at each of the four shear orientations. Each panel shown is at the time of maximum low-level vertical vorticity.

$$C = \sqrt{-2 \int_0^H B\, dz} \tag{4.4}$$

The 180° case appears to have the strongest cold pool intensity in the vicinity of the midlevel mesocyclone along each of the three shear layer depths despite having less outflow directly below the midlevel mesocyclone. The other runs appear to be relatively similar when looking at the snapshot of cold pool intensity. Figures 4.16, 4.17, and 4.18 show a cross-section of the cold pool through the maximum updraft

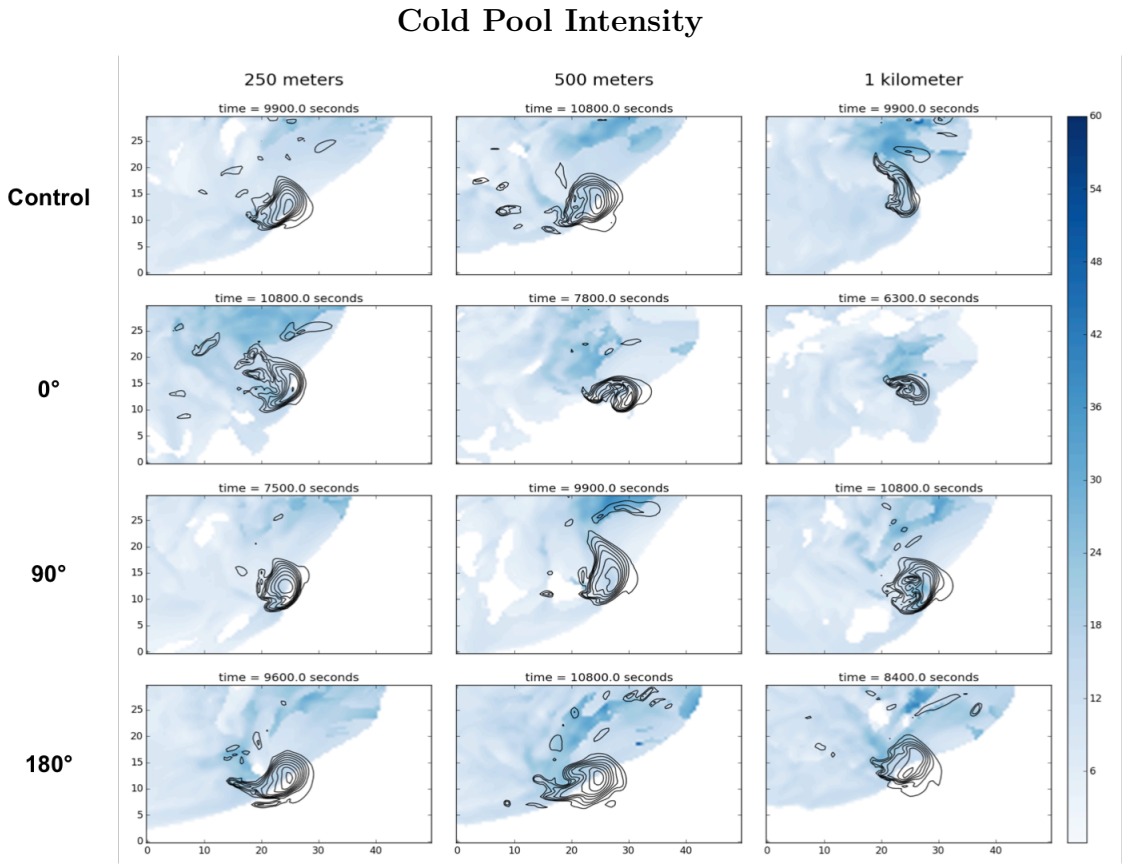


Figure 4.15: Cold pool intensity at time of maximum low-level vertical vorticity for each simulation run.

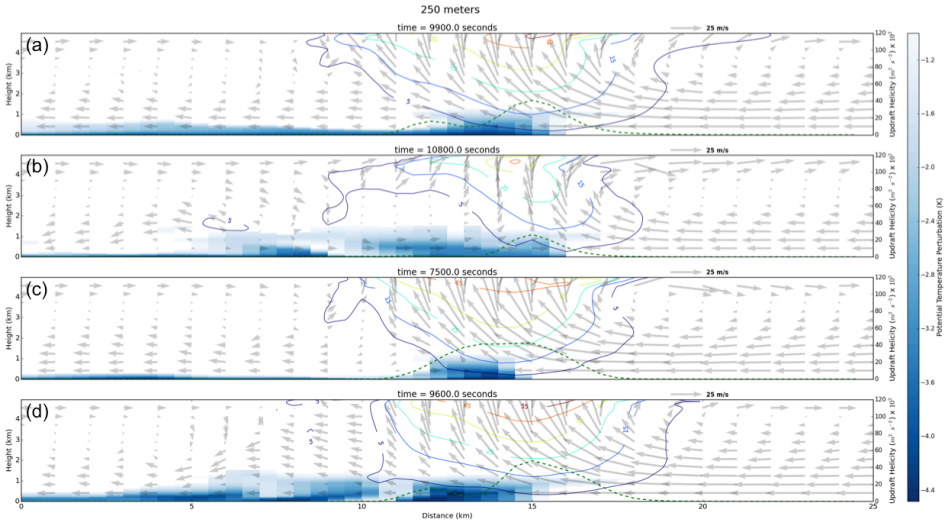


Figure 4.16: Cold pool cross-section at time of maximum low-level vertical vorticity for **(a):** CTL-250M-7MS, **(b):** 0DEG-250M-7MS, **(c):** 90DEG-250M-7MS, and **(d):** 180DEG-250M-7MS. The cross-section is taken through the maximum updraft helicity. The blue shaded region is the potential temperature perturbation, the contours are the updraft intensity plotted every 10 m $s^{-1}$, the dotted green line is the maximum updraft helicity, and the arrows are the u and w components of the winds. The values of the maximum updraft helicity can be seen on the axis on the right and point to the value at the each x location.

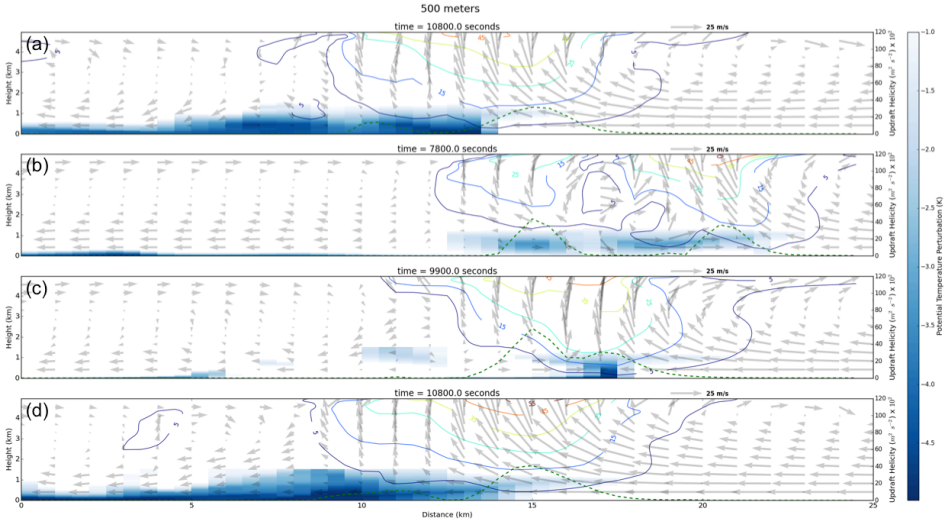


Figure 4.17: Same as Figure 4.16, but for 500-meter shear layer depth.

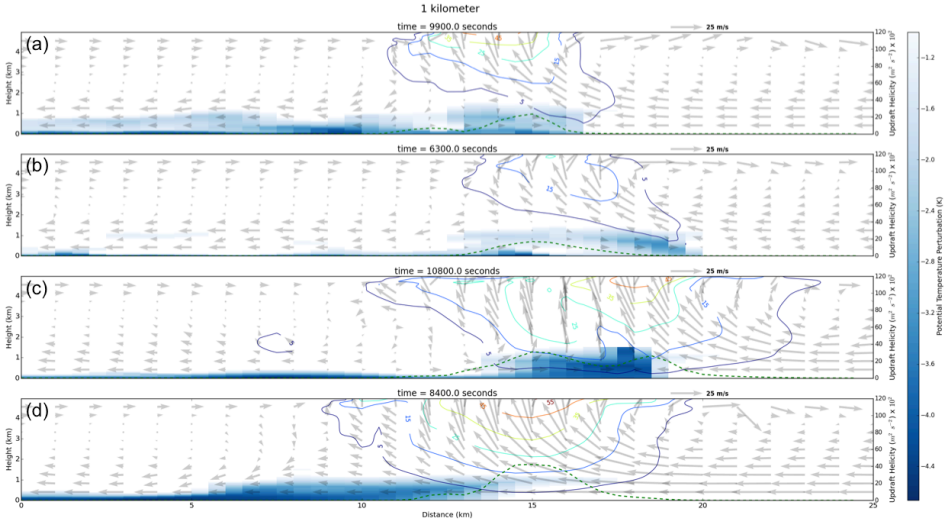


Figure 4.18: Same as Figure 4.16, but for 1 kilometer shear layer depth.

helicity. This shows a clearer picture of how the winds are affecting the cold pool. Through each simulation the 0° case appears to have the weakest cold pool and is also the furthest east compared to the other angles. On the other hand the 180° cases appear to be the strongest, but they are held back behind the updraft.

The lowest cold pool intensity appears in the 90° cases, with the 0° case landing in the center of them all. 0DEG-1KM-7MS has the most cold pool surrounding the midlevel mesocyclone, much more than any of the other runs. This can be seen in Figure 4.19. In fact, all the 0° cases have a large area of cold pool intensity, while the 180° cases, which have the strongest cold pool intensity, have the least amount of area with cold pool beneath the midlevel mesocyclone. Changing the critical angle of the low-level wind shear has an effect on the cold pool because of the gust front relative winds over the depth of the cold pool. In spite of the strength of the cold

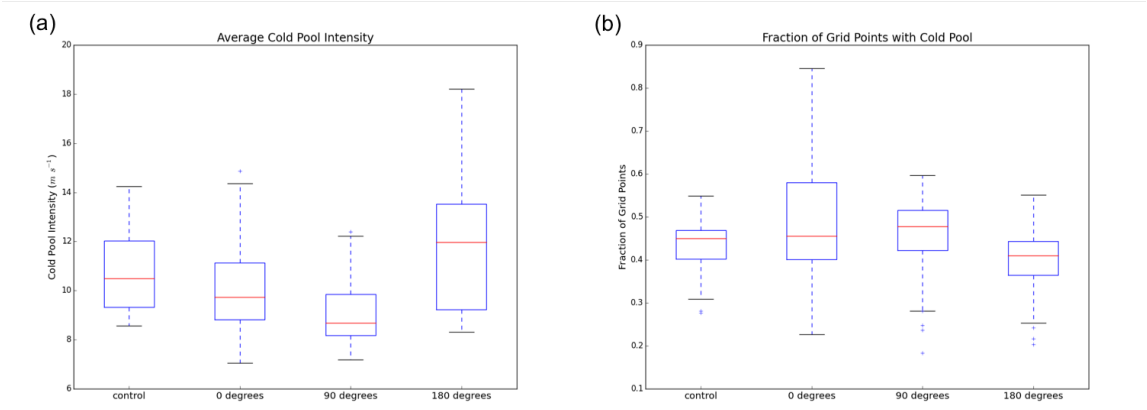


Figure 4.19: **(a):** Box and whiskers plot of the average cold pool intensity (excluding areas without cold pool) over a 25 x 17.5 km area determined by the position of the maximum updraft helicity categorized by angle. **(b):** Box and whiskers plot of the fraction of grid points with cold pool, within the 25 x 17.5 km box, categorized by angle. Excludes the first hour.

pool, the gust front relative winds appear to have the greater control. In 180DEG-500M-7MS, even though it has a strong cold pool, which should cause the outflow to surge forward, the outflow remains restrained behind the storm due to the gust front relative winds.

Figure 4.20 shows the correlation between the average cold pool intensity and the distance between the midlevel mesocyclone and the maximum near-ground circulation. 0° and 90° have a p-value above 0.01, meaning they are not statistically significant. The total correlation is statistically significant, but the correlation is only -0.32. The largest value is the control with a correlation of -0.60, which means there is a high correlation between the cold pool intensity and the distance where no low-level wind shear is present. There is some negative correlation between the cold pool intensity and the distance, but it is much smaller than the correlation between

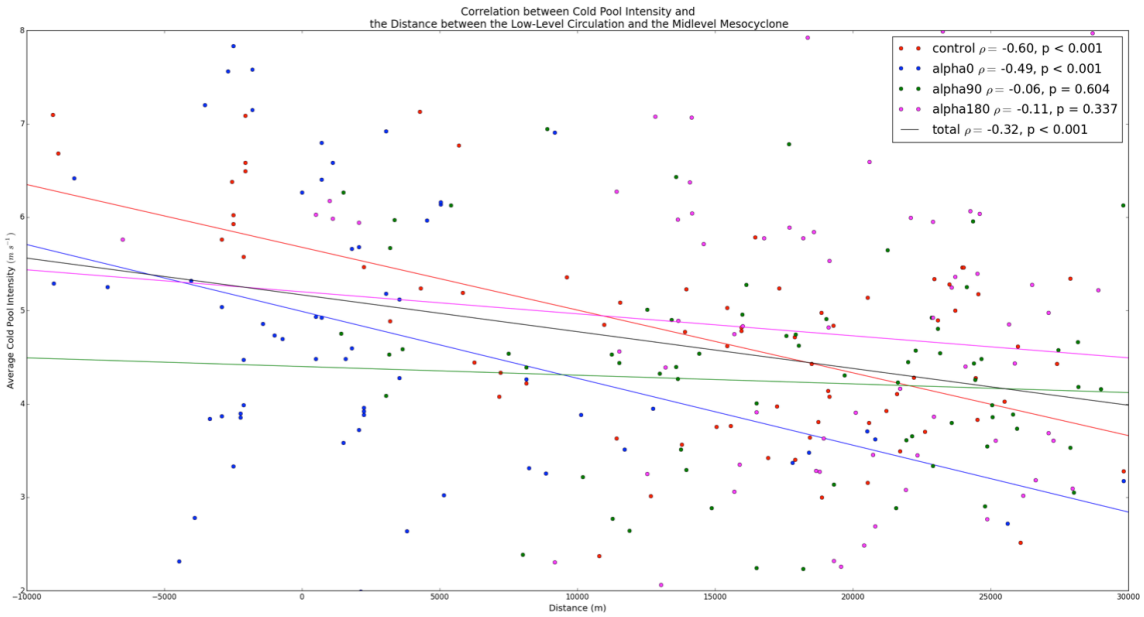


Figure 4.20: Correlation between Distance and cold pool intensity, separated by critical angle.

the vertical vorticity and the circulation.

# 5 SUMMARY AND CONCLUSIONS

In this study, focus was placed on the effects of low-level wind shear orientation, depth, and magnitude on the near-ground rotation in a simulated supercell thunderstorm. It was hypothesized that the low-level shear would affect the position of the near-ground, circulation-rich outflow relative to the overlying midlevel mesocyclone. That position, in turn, would affect the corresponding vertical vorticity.

In order to test this hypothesis the numerical model CM1 was used to run idealized simulations of supercell thunderstorms. The thermodynamics of each simulation remained the same while the wind profile varied. Several sets of simulations were run including three shear layer depths (250-meter, 500-meter, and 1 km) and two shear layer magnitudes (7 m $s^{-1}$ and 15 m $s^{-1}$). Each of these case was run with a control (no shear) case and three different shear orientations (0°, 90° and 180°). Each simulation was run for 3 hours and had output every 5 minutes.

Several questions were posed regarding the influence of low-level shear on rotation in supercell thunderstorms:

1. How does the direction, magnitude, and strength of low-level shear affect the magnitude of near-ground rotation?

   There was a relationship seen between the low-level shear orientation and the magnitude of the near-ground rotation. In each case, the trends remained the same, although they were either magnified or subdued based on the shear

depth and magnitude. 0DEG-500M-7MS and 0DEG-250M-7MS had the largest maximum circulation below the midlevel mesocyclone, while CTL-1KM-7MS had the largest for the 1 kilometer shear layer runs.

There was hardly any near-ground rotation when the shear magnitude was raised to 15 m $s^{-1}$. The trend were amplified so much so that there was very little of no near-ground circulation.

2. Do changes in the low-level shear orientation, strength, and depth affect the properties and/or the positioning of supercell outflow relative to the midlevel mesocyclone?

   Again, trends are seen with the orientation of low-level shear and the position of the outflow. The 0° cases push the outflow in an easterly direction. In the case of 0DEG-500M-7MS and 0DEG-250M-7MS this aligns the edge of the outflow with the midlevel mesocyclone. When the shear layer is increased to 1 kilometer or the magnitude is amplified, the orientation of the shear layer has a larger effect, causing the outflow to surge out ahead of the midlevel mesocyclone.

   This pattern is seen in the other simulations as well. In every simulation the 180° case sees the outflow restrained behind the midlevel mesocyclone. 90DEG-500M-7MS and 90-250M-7MS has the outflow aligning with the midlevel mesocyclone towards the end of the run. CTL-1KM-7MS is the only case where the control outflow is aligned with the midlevel mesocyclone. All the other control

cases have the outflow behind the storm.

3. Does this relative positioning influence the strength of near-ground rotation?

   Finally, there is a statistically significant correlation between the position of the outflow relative to the midlevel mesocyclone and the strength of the near-ground circulation. Surface vertical vorticity was generally strongest when the distance between the midlevel mesocyclone and the maximum surface circulation was relatively small. In each simulation, the near-ground circulation became stronger when the distance decreased.

One result that came about that was not expected was how much effect the 250-meter shear layer had on the simulated supercells. Previous studies (e.g., Brooks and Craven 2002, Markowski et al. 2003, Thompson et al. 2003) have shown that a low-level shear layer of 1 kilometer is ideal for discriminating between tornadic and nontornadic supercells, but it might be that even shallower layers could have an impact. It would be interesting to look into shallower layers in future work.

Overall, 0° appears to be the best orientation for supercell tornadogenesis in this study with the parameters used. This is different from the findings of Esterheld and Giuliano (2008), who looked at actual tornadic supercell cases and found that 90° orientation appeared the most frequently. There are many factors, however, that could play into this difference: the magnitude of the low-level wind shear, the depth over which the orientation was calculated, and even the LCL. There are also several factors left out of this study's simulations, such as: radiation, surface friction, coriolis

force, terrain etc. It is possible that if these parameters were added in this study could come to the same conclusions as Esterheld and Giuliano (2008).

The conclusions presented herein also differ from those presented in Frame and Markowski (2013). In their study, Frame and Markowski (2013) simulated supercell thunderstorms using the Advanced Regional Prediction System (ARPS) model. They included surface fluxes, radiative transfer, and a soil model in their simulations, unlike the simulations presented herein. When these parameters are included and anvil shading is applicable, Frame and Markowski (2013) found that easterly shear is actually detrimental to the storm. Without the anvil shading, however, their simulations showed that easterly shear actually strengthened the storms.

It is clear from the differences seen between this research and previous studies that more parameters need to be taken into account (e.g. surface fluxes, radiation, surface friction, etc.). There is also a fair amount of future work to be done before the effects of low-level wind shear can be fully understood. Some suggestions would be:

1. Run similar simulations with decreased low-level wind shear as well as similar simulations for a semi-circle hodograph.

   In this study the hodograph structure used was quarter-circle, clockwise turning with unidirectional westerly shear above 2 km. While this is an ideal hodograph structure for supercells, a semi-circle hodograph has also been shown be an ideal set-up for the formation of supercells (Weisman and Klemp, 1984). How would

the findings in this study compare to one with a semi-circle hodograph?

2. Compare results to real tornadic supercell cases to validate findings.

   Numerical simulations are a powerful tool to use in research studies, but if the results presented herein are not seen in the actual atmosphere, there is not much that can be said about them. In order for these results to be fundamental to the tornado forecasting process, they must be validated and proven true.

3. Investigate the hypothesis that LCL may play a role in supercell tornadogenesis by modifying the intensity and position of outflow relative to the overlying mesocyclone.

   LCL has also been shown to be a significant predictor for tornadic supercells and thus cannot be ignored. There may be an optimized balance between the low-level shear and the LCL, which gives the greatest chance of a tornadic supercell. While in this study the 0° case was found to be optimal, it is possible that with changing LCL, that might not be the case.

The findings in this study are a good start to better understanding tornadogenesis and its ideal environment. While this study only tested a few cases with a single hodograph, the results are still promising. These results imply a connection between low-level shear orientation and strength of near-ground rotation. While these results cannot be directly applied to our atmosphere and contradict some previous studies, they do show that there is a connection between the shear orientation and the intensification of near-ground rotation. Markowski and Richardson (2014) showed

that the strength of the dynamic forcing in important to tornadogenesis, but the positioning also appears to be important as well and driven by the orientation of the wind shear. Forecasters should look not only at the magnitude of low-level shear, but also the orientation to get a better feel for tornadic supercell predictions.

# REFERENCES


Ahrens, C., 2009: *Meteorology Today: An introduction to weather*. 9th ed., Brooks/Cole, Belmont, CA.

Benjamin, S. G., and Coauthors, 2016: A north american hourly assimilation and model forecast cycle: The rapid refresh. *Mon. Wea. Rev.*, **144**, 1669–1694.

Brooks, H., and J. Craven, 2002: A database of proximity soundings for significant severe thunderstorms. Preprints, *21st Conf. on Severe Local Storms*, San Antonio, TX, Amer. Meteor. Soc.

Browning, K. A., 1964: Airflow and precipitation trajectories within severe local storms which travel to the right of the winds. *J. Atmos. Sci.*, **21**, 634–639.

Browning, K. A., and F. H. Ludlam, 1962: Airflow in convective storms. *J. Atmos. Sci.*, **88**, 117–135.

Bryan, G. H., 2012: What is rkw theory? *26th Conf. on Severe Local Storms*, Nashville, TN, NCAR, [Available online at http://www2.mmm.ucar.edu/people/bryan/Presentations/Bryan_SLS_2012.pdf.].

Bryan, G. H., 2014: The governing equations for cm1. [Available online at http://www2.mmm.ucar.edu/people/bryan/cm1/].

Bryan, G. H., and J. M. Fritsch, 2002: A benchmark simulaiton for moist nonhydrostatic numerical models. *Mon. Wea. Rev.*, **130**, 2917–2928.

Bunkers, M. J., B. A. Klimowski, J. W. Zeitler, R. L. Thompson, and M. L. Weisman, 2000: Predicting supercell motion using a new hodograph technique. *Wea. Forecasting*, **15**, 61–79.

Coffer, B., and M. D. Parker, 2015: Impacts of increasing low-level shear on supercell during the early evening transition. *Mon. Wea. Rev.*, **143**, 1945–1969.

Craven, J. P., and H. E. Brooks, 2004: Baseline climatology of sounding derived parameters associated with deep, moist convection. *Natl. Weather Dig.*, **28**, 13–24.

Cutter, S. L., Ed., 2001: *American hazardscapes: The regionalization of hazards and disasters*. Joseph Henry Press, Washington, DC.

Dahl, J. M. L., M. D. Parker, and L. J. Wicker, 2014: Imported and storm-generated near-ground vertical vorticity in a simulated supercell. *J. Atmos. Sci.*, **71**, 3027–3051.

Davies-Jones, R., 1982: A new look at the vorticity equation with application to tornadogenesis. Preprints, *12th Conf. on Severe Local Storms*, San Antonio, TX, AMS, 249–252.

Davies-Jones, R., 1984: Streamwise vorticity: The origin of updraft rotation in supercell storms. *J. Atmos. Sci.*, **41**, 2991–3006.

Davies-Jones, R., 2006: Tornadogenesis in supercells: What we know and what we don't know. Preprints, *23rd Conf. on Severe Local Storms*, San Antonio, TX, Amer. Meteor. Soc.

Davies-Jones, R., D. Burgess, and M. Foster, 1990: Test of helicity as a tornado forecast parameter. Preprints, *16th Conf. on Severe Local Storms*, Kananaskis Park, AB, Canada, AMS, 588–592.

Davies-Jones, R., R. J. Trapp, and H. B. Bluesmen, 2001: Tornadoes and tornadic storms. *Severe Convective Storms*, 167–221.

Deardorff, J. W., 1980: Stratocumulus-capped mixed layers derived from a three-dimensional model. *Bound.-Layer Meteor.*, **18**, 495–527.

Durran, D. R., and J. B. Klemp, 1983: A compressible model for the simulation of moist mountain waves. *Mon. Wea. Rev.*, **111**, 2341–2361.

Edwards, R., 2000: The online tornado faq: Frequently asked questions about tornadoes. [Available online at http://www.spc.noaa.gov/faq/tornado/].

Esterheld, J. M., and D. J. Giuliano, 2008: Discriminating between tornadic and non-tornadic supercells: A new hodograph technique. *E-Journal of Severe Storms Meteorology*, **3**, 1–50.

Frame, J., and P. Markowski, 2013: Dynamical influences of anvil shading on simulated supercell thunderstorms. *Mon. Wea. Rev.*, **141**, 2802–2820.

Grasso, L. D., and W. R. Cotton, 1995: Numerical simulation of a tornado vortex. *J. Atmos. Sci.*, **52**, 1192–1203.

James, R. P., P. M. Markowski, and J. M. Fritsch, 2006: Bow echo sensitivity to ambient moisture and cold pool strength. *Mon. Wea. Rev.*, **134**, 950–964.

Johns, R. H., and C. A. Doswell, 1992: Severe local storms forecasting. *Wea. Forecasting*, **7**, 588–612.

Klemp, J. B., 1987: Dynamics of tornadic thunderstorms. *Annu. Rev. Fluid Mech.*, **19**, 369–402.

Klemp, J. B., and R. B. Wilhelmson, 1978: The simulation of three-dimensional convective storm dynamics. *J. Atmos. Sci.*, **35**, 1070–1096.

Klemp, J. B., R. B. Wilhelmson, and P. S. Ray, 1981: Observed and numerically simulated structure of a mature supercell thunderstorm. *J. Atmos. Sci.*, **38**, 1558–1580.

Lemon, L. R., and C. A. Doswell, 1979: Severe thunderstorm evolution and mesocyclone structure as related to tornadogenesis. *Mon. Wea. Rev.*, **107**, 1184–1197.

Lilly, D. K., 1979: The dynamical structure and evolution of thunderstorms and squall lines. *Annu. Rev. Earth and Planetary Sciences*, **7**, 117–161.

Lilly, D. K., 1982: The development and maintenance of rotation in convec-

tive storms. *Intense Atmospheric Vortices*, L. Bengtsson, and J. Lighthill, Eds., Springer Berlin Heidelberg, 149–160.

Mansell, E. R., 2010: On sedimentation and advection in multimoment bulk microphysics. *J. Atmos. Sci.*, **67**, 3084–3094.

Markowski, P., C. Hannon, J. Frame, E. Lancaster, A. Pietrycha, R. Edwards, and R. L. Thompson, 2003: Characteristics of vertical wind profiles near supercells obtained from the rapid update cycle. *Wea. Forecasting*, **18**, 1262–1272.

Markowski, P., and Y. P. Richardson, 2009: Tornadogenesis: Our current understanding, forecasting considerations, and questions to guide future research. *Atmospheric Research*, **93**, 3–10.

Markowski, P., and Y. P. Richardson, 2011: *Mesoscale Meteorology in Midlatitudes*. John Wiley & Sons, Hoboken, NJ.

Markowski, P., and Y. P. Richardson, 2014: The influence of environmental low-level shear and cold pools on tornadogenesis: Insights from idealized simulations. *J. Atmos. Sci.*, **71**, 243–275.

Markowski, P., E. R. J. Straka, R. Davis-Jones, Y. Richardson, and R. J. Trapp, 2008: Vortex lines within low-level mesocyclones obtained from pseudo-dual-doppler radar observations. *Mon. Wea. Rev.*, **136**, 3513–3535.

Moller, A. R., C. A. Doswell, M. P. Foster, and G. R. Woodall, 1994: The operational

recognition of supercell thunderstorm environments and storm structures. *Wea. Forecasting*, **9**, 327–347.

Morrison, H., J. A. Curry, and V. I. Khvorostyanov, 2005: A new double-moment microphysics parameterization for application in cloud and climate models. part i: Description. *J. Atmos. Sci.*, **62**, 1665–1677.

Parker, M., 2014: Composite vortex2 supercell environments from near-storm soundings. *Mon. Wea. Rev.*, **142**, 508–529.

Rasmussen, E. N., and D. O. Blanchard, 1998: A baseline climatology of sounding-derived supercell and tornado forecast parameters. *Wea. Forecasting*, **13**, 1148–1164.

Rogers, R. R., and M. Yau, 1989: *A short course in cloud physics, International series in natural philosophy*. 3rd ed., Elsevier, Burlington, MA.

Rotunno, R., 1981: On the evolution of thunderstorm rotation. *Mon. Wea. Rev.*, **109**, 577–586.

Rotunno, R., and J. Klemp, 1985: Simulation and analysis of tornado development and decay within a three-dimensional supercell thunderstorm. *J. Atmos. Sci.*, **42**, 271–292.

Rotunno, R., J. B. Klemp, and M. L. Weisman, 1988: A theory for strong, long-lived squall lines. *J. Atmos. Sci.*, **45**, 463–485.

Thompson, R. L., and R. Edwards, 2000: An overview of environmental conditions and forecast implications of the 3 may 1999 tornado outbreak. *Wea. Forecasting*, **15**, 682–699.

Thompson, R. L., R. Edwards, J. A. Hart, K. L. Elmore, and P. Markowski, 2003: Close proximity soundings within supercell environments obtained from the rapid update cycle. *Wea. Forecasting*, **18**, 1243–1261.

Trapp, R. J., G. J. Stumpf, and K. L. Manross, 2005: A reassessment of the percentage of tornadic mesocyclones. *Wea. Forecasting*, **20**, 680–687.

Weisman, M. L., and J. B. Klemp, 1982: The dependence of numerically simulated convective storms on vertical wind shear and buoyancy. *Mon. Wea. Rev.*, **110**, 504–520.

Weisman, M. L., and J. B. Klemp, 1984: The structure and classification of numerically simulated convective stormsin directionally varying wind shears. *Mon. Wea. Rev.*, **112**, 2479–2498.

Weisman, M. L., and J. B. Klemp, 1986: Characteristics of isolated convective storms. *Mesoscale Meteorology and Forecasting*, 331–358.

Weisman, M. L., and R. Rotunno, 2000: The use of vertical wind shear versus helicity in interpreting supercell dynamics. *J. Atmos. Sci.*, **57**, 1452–1472.

Weisman, M. L., and R. Rotunno, 2004: A theory for strong long-lived squall lines" revisited. *J. Atmos. Sci.*, **61**, 361–382.